ORGANOMETALLICS

pubs.acs.org/Organometallics Article

Synthesis and Structure of P-Halogenated Benzazaphospholes and Their Reactivity toward Pt(0) Sources

Preston M. Miura-Akagi, Timothy W. Chapp, Wesley Y. Yoshida, Glenn P. A. Yap, Arnold L. Rheingold, Russell P. Hughes,* and Matthew F. Cain*

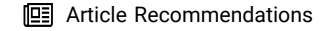


Cite This: Organometallics 2023, 42, 672-688

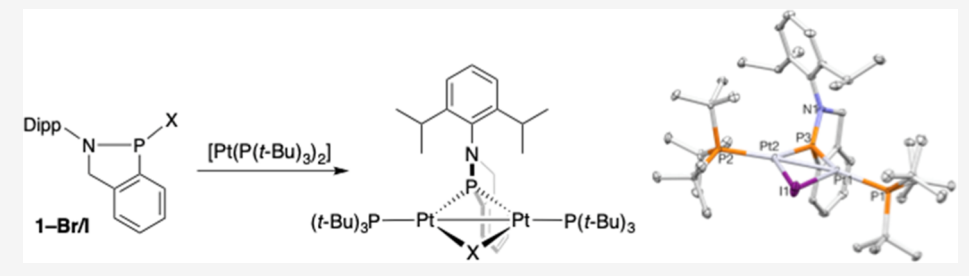


ACCESS I

III Metrics & More



SI Supporting Information



ABSTRACT: Dearomatization of the five-membered ring of N-Dipp (Dipp = 2,6-diisopropylphenyl)-substituted benzazaphosphole 2 with HCl generated 1-Cl, which undergoes substitution with halide sources to provide the remaining members of the Phalogenated series (1-F, 1-Br, and 1-I). These P-heterocycles (1) were characterized by multinuclear [31P{1H}, 1H, 13C{1H}, and 19 F (if applicable)] NMR spectroscopy, elemental analysis, and X-ray crystallography. 1 H and 13 C 1 H} NMR spectroscopy revealed that derivatives 1-F, 1-Cl, and 1-Br have C_1 symmetry in solution. In contrast, 1-I has effective C_2 symmetry in solution due to a rapid, concentration-dependent, inversion at phosphorus, shown by density functional theory (DFT) calculations (B3LYP-D3/6-311 $G^{**}++$) to involve a dimeric iodine-bridged transition structure. In the solid state, 1-F through 1-I all exhibited C_1 symmetry with varying degrees of elongation of their P-X bonds. Elongation of the P-X bonds is shown by DFT/natural bond orbital studies to involve $N_{LP} \to \sigma^*(P-X)$ negative hyperconjugation, which increases down the halogen series but is less pronounced than that for the closely related NHP-X counterparts (3-F through 3-I). Treatment of 1-Br/I with $[Pt(P(t-Bu)_3)_2]$ afforded Pt(I)-Pt(I)dimers 4-Br/I, which were characterized by ³¹P{¹H}, ¹H, and ¹³C{¹H} NMR spectroscopy, elemental analysis, and X-ray crystallography. Addition of 1-F to Pt(PPh₃)₄ gave Pt(1-F)(PPh₃)₂ (6), a coordination compound in which the P-heterocyclic ligand is bound through its lone pair without P-F bond cleavage. Recrystallization attempts resulted in ligand exchange, furnishing Pt(0) complex 7, which features 1-F and PPh3 donors in a 2:1 ratio. Reactions of 1-Cl with all tested starting materials produced unidentifiable product mixtures by ${}^{31}P{}^{1}H}$ NMR spectroscopy, but the combination of $Pt(PPh_3)_4$ or $Pt(PPh_3)_2(C_2H_4)$ and 1-Cl in acetone generated an unisolable Pt complex containing tentatively assigned PtP2 metallacyclopropane structural unit 8.

■ INTRODUCTION

When the chemical properties of phosphorus and carbon mirror each other, chemists often invoke their diagonal relationship on the periodic table of elements, even referring to phosphorus as a "carbon copy". However, if they are accessible, the structure and bonding of P-based building blocks can differ greatly from their organic analogues. For example, phosphenium ions (PR2+) are isoelectronic with carbenes $(CR_2)^2$, but the parent PH_2^+ is a singlet with a H-P-H bond angle approaching 90 deg,³ while CH₂ is sp²hybridized with a triplet ground state (Figure 1, left).^{4,5} The introduction of flanking amino substituents to both these reactive intermediates renders them isolable, 6 leading to their common description as NHPs (N-heterocyclic phospheniums or phosphines)⁷ and NHCs (N-heterocyclic carbenes),⁸ respectively. The π -donation from the N lone pairs in an NHC drives up the energy of the lowest unoccupied molecular orbital (LUMO),⁵ affording a singlet carbene that acts as a potent σ -donor to transition-metal complexes.⁸ Exchange of one of the sp²-hybridized N atoms for an sp³-hybridized carbon center gives a cyclic (alkyl)(amino)carbene (CAAC),⁹ which acts as both a better σ -donor (higher highest occupied molecular orbital, HOMO) and π -acceptor (lower LUMO) to a metal center than an NHC.¹⁰ In fact, the small HOMO–LUMO gap in a CAAC enables ambiphilic reactivity,¹¹ resulting in E–H bond activation (E = H, H₂N, etc.) at carbon.¹² By swapping the sp³-hybridized carbon for a fused

Received: January 31, 2023 Published: April 4, 2023



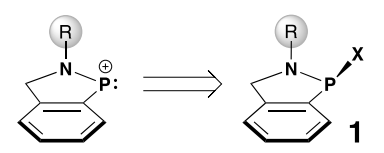


Figure 1. Electronic configuration (left) and structure of specific classes of phosphenium ions and carbenes (right).

and more electron-withdrawing sp²-hybridized phenyl substituent, the HOMO–LUMO gap can be further reduced, but the cyclic (amino)(aryl)carbene (CAArC) is unisolable and must be trapped at low temperature.¹³ The predicted structure of the CAArC revealed that the angle at the carbene carbon would be more acute than a CAAC, so we speculated that this type of strained five-membered ring may be more stable if the sp²-hybridized C was replaced by an unhybridized P+ while simultaneously retaining the small HOMO–LUMO gap necessary for small-molecule activation (Figure 1, right).¹⁴

While phosphenium ions are commonly generated via halide abstraction from their P-halogenated precursors, 15,16 until recently, precursors featuring a P-center confined in a five-membered ring by a neighboring π -donating N-substituent and sp²-hybridized benzene with an exocyclic P–X bond (X = halogen) were unknown (Scheme 1). However, during the

Scheme 1. Potential Retrosynthetic Pathway to Phosphenium Ions Derived from P-Halogenated Benzazaphospholes 1 (X = Halogen)



development of P-alkynyl transmetalating agents, 1-Cl and 1-I were synthesized. Despite only a difference in the identity of the halogen, NMR studies illustrated that 1-Cl had the expected C_1 symmetry in solution, while the broad spectrum of 1-I led to the suggestion that it might be ionic. 18 Since NHPs (structure shown above in Figure 1) are accessed in wideranging yields from their corresponding chloro, 2,19 bromo, 16b and iodo²⁰ precursors using a variety of Lewis acids or directly via a one-step redox process with diimines and PI₃, ²¹ we sought a more complete understanding of the structure, bonding, and reactivity of the entire series of P-halogenated derivatives of 1-X and their relationships to the corresponding phosphenium cations (Scheme 1). Here, we describe the synthesis and crystallographic characterization of the remaining fluoro (1-F) and bromo (1-Br) analogues, analysis of their structures in solution by NMR spectroscopy and computationally with density functional theory (DFT) calculations, and document the reactivity of these P-halogenated species toward Pt(0).

RESULTS AND DISCUSSION

Synthesis and Structures of Dearomatized and P-Halogenated Benzazaphospholes (1). Dearomatization of the five-membered ring of *N*-Dipp (Dipp = 2,6-diisopropyl-

phenyl)-substituted benzazaphosphole²² **2** with HCl afforded **1**–Cl,¹⁸ which has been previously characterized by NMR spectroscopy, elemental analysis, and X-ray crystallography. Given that **1**–Cl served as an excellent precursor to iodo analogue **1**–**I** via its treatment with trimethylsilane (TMS)–I,²³ we hypothesized that related substitution reactions would generate **1**–**F** and **1**–**Br**, respectively (Scheme 2).

Scheme 2. Synthesis of 1-F, 1-Cl, 1-Br, and 1-I

Indeed, exposure of 1-Cl to CsF/TMSCF₃ (1:2 ratio)²⁴ furnished fluorinated 1-F, readily identified by 31P{1H} NMR spectroscopy as a prominent doublet (δ 150.1 and J_{PF} = 1035 Hz). The ¹⁹F and ¹H NMR spectra of 1–F highlighted its C₁-symmetric structure featuring a P-stereocenter and diastereotopic benzylic protons. In the ¹⁹F NMR spectrum, a doublet of doublets of doublets ($J_{PF} = 1035 \text{ Hz}$, $J_{HF} = 28 \text{ Hz}$, and $J_{\rm HF}$ = 19 Hz) was observed at -81.0 ppm, reflecting the inequivalent nature of CH2 protons. These same CH2 protons resonated as doublets of doublets of doublets in the ¹H NMR spectrum at 4.83 and 4.17 ppm. In the case of the more downfield shifted signal (δ 4.83), its largest J (J_{HF} = 28 Hz) is greater than the sum of the remaining two J values ($J_L \ge J_M +$ J_S ; 28 \geq 16 + 5; L = large, M = medium, and S = small), and therefore, its splitting pattern is consistent with that of a traditional ddd. However, the upfield shifted signal (δ 4.17) has the opposite situation, i.e, the largest $J(J_{HF} = 19 \text{ Hz})$ is less than the sum of the remaining two J values $(J_L \leq J_M + J_S; 19 \leq$ 16 + 13.5), resulting in a ddd with an unusual appearance (Figure 2).

Additionally, the ¹H NMR spectrum of **1**–F displayed four methyl and two methine resonances, indicative of a pyramidal phosphorus stereocenter and an orthogonally aligned *N*-Dipp substituent with restricted rotation. The ¹³C{¹H} NMR spectrum also supported this assignment as 12 aryl resonances (six for Dipp and six for the fused benzene ring) were

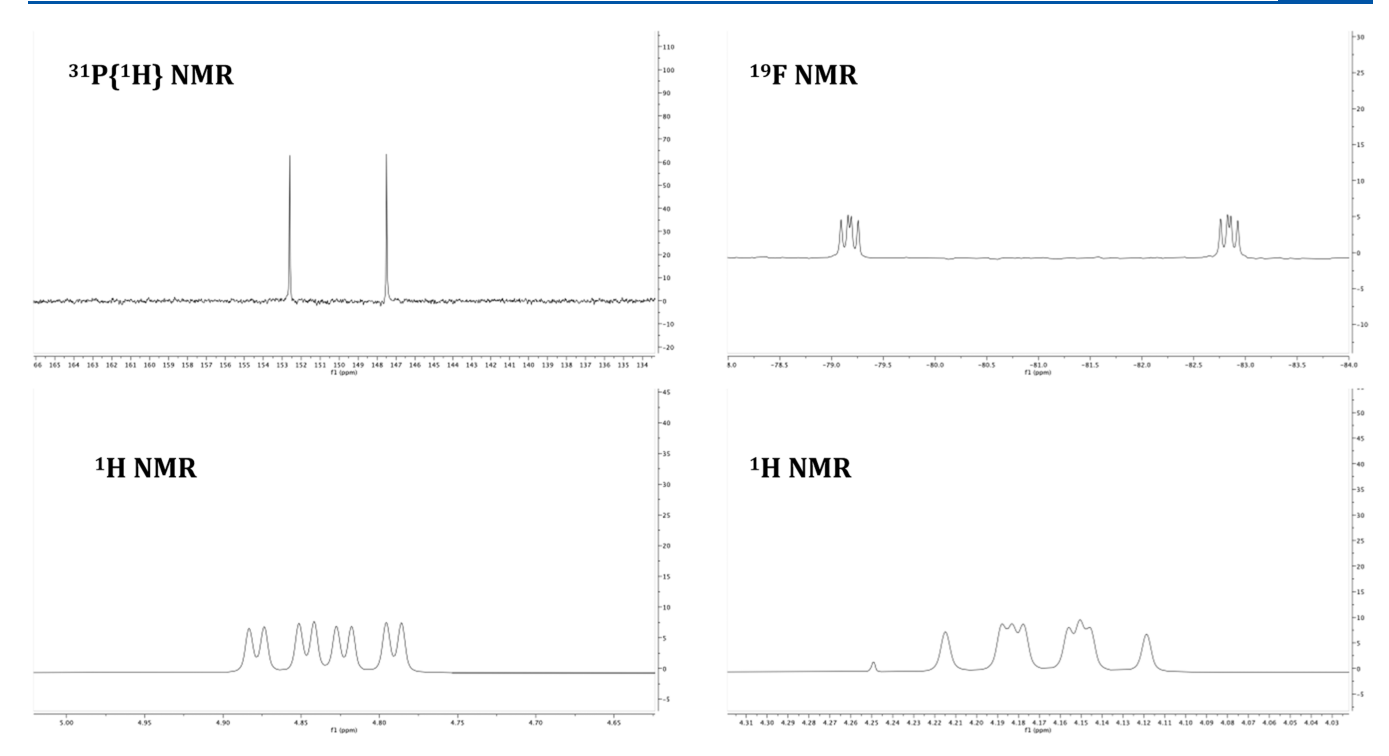


Figure 2. Key NMR spectroscopic data for 1–F. Upper left: ${}^{31}P\{{}^{1}H\}$ NMR; upper right: ${}^{19}F$ NMR; lower left: a selected region of the ${}^{1}H$ NMR spectrum showing one of the diastereotopic CH₂ protons; and lower right: a selected region of the ${}^{1}H$ NMR spectrum displaying the other diastereotopic CH₂ proton. The singlet at 4.25 ppm is trace DCM.

observed. Ultimately, the structure and bulk purity of 1-F was confirmed by X-ray crystallography and elemental analysis (Figure 3). The solid-state structures of the heavier halogen analogues are also of C_1 symmetry and are discussed later.

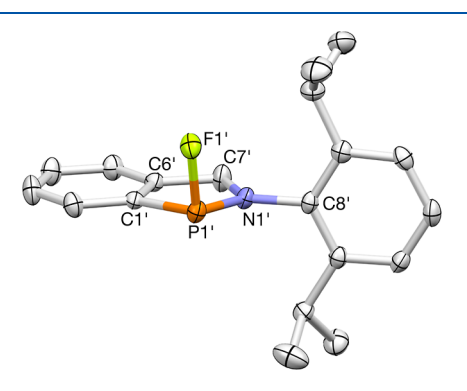


Figure 3. X-ray crystal structure of one of the two independent molecules of 1–F. Selected bond lengths (Å) and angles (deg): $P_1{}^{\prime}-F_1{}^{\prime}=1.6569(15),\; P_1{}^{\prime}-N_1{}^{\prime}=1.6716(15),\; P_1{}^{\prime}-C_1{}^{\prime}=1.8178(18),\; N_1{}^{\prime}-C_7{}^{\prime}=1.471(2),\; C_1{}^{\prime}-P_1{}^{\prime}-N_1{}^{\prime}=89.23(8),\; F_1{}^{\prime}-P_1{}^{\prime}-N_1{}^{\prime}=104.24(8),\; \text{and}\; F_1{}^{\prime}-P_1{}^{\prime}-C_1{}^{\prime}=96.95(8).$

In a similar fashion to 1–I, treatment of 1–Cl with TMS–Br afforded 1–Br, 24 which contained a $^{31}P\{^{1}H\}$ NMR signal at 157 ppm (Scheme 2, above). At 20 °C, ^{1}H NMR spectroscopy revealed that the structure of 1–Br had C_{1} -symmetry exemplified by its diastereotopic benzylic protons (δ 4.89 and 3.98) and two distinct methine and four methyl signals, corresponding to the inequivalent i-Pr protons on the rotationally locked N-Dipp substituent, and consistent with the solid-state structure (vide infra); however, all of the resonances were somewhat broadened. In the case of 1–I, 18 which has an analogous solid-state structure, the room-

temperature 1H NMR spectrum (Figure 4) was extremely broad, and a single peak for the CH_2 protons with a sole methine resonance and two methyl signals for the i-Pr groups was observed, demonstrating that 1-I had effective C_s symmetry, while at lower temperatures, the spectrum sharpened with decoalescence to a C_1 -symmetric structure. This variable temperature behavior is only consistent with a low energy inversion of stereochemistry at the chiral phosphorus. 27

This inversion of configuration can occur via sp²- (vertex inversion)²⁸ or square planar-type (edge inversion)²⁹ transition structures with the latter favored for phosphines containing π -donors like the amino and halogenated substituents on 1 (see graphic in Table 1).³⁰ DFT calculations (Table 1) predict that edge inversion of the P-center is indeed preferred in all P-heterocycles 1–X, but the barriers are too high for P-inversion to be relevant on the NMR time scale. Vertex inversion required application of geometry constraints to the transition structures, so they do not represent stationary points and their energies are still substantially higher.

With P-inversion ruled out, the original postulate that the VT NMR spectroscopic observations might be a consequence of ionic character or bond strengths of 1–X, with dissociation of Br⁻ or I⁻ anions being responsible for the NMR behavior, was reexamined, although such behavior is unlikely in the nonpolar solvent used. Indeed, natural bond orbital (NBO) studies of the P–X bonds in compounds 1–X and both their homo- and heterolytic bond dissociation free energies (Table 2) are inconsistent with this hypothesis. Not unexpectedly, the ionic character and the strength of the P–X bonds decrease from F to I, but even the weakest bond is insufficient to account for the rapidity of the NMR timescale process.

Exploration of alternative pathways by DFT led to the bimolecular pathway shown in Figure 5 (top, schematic). A

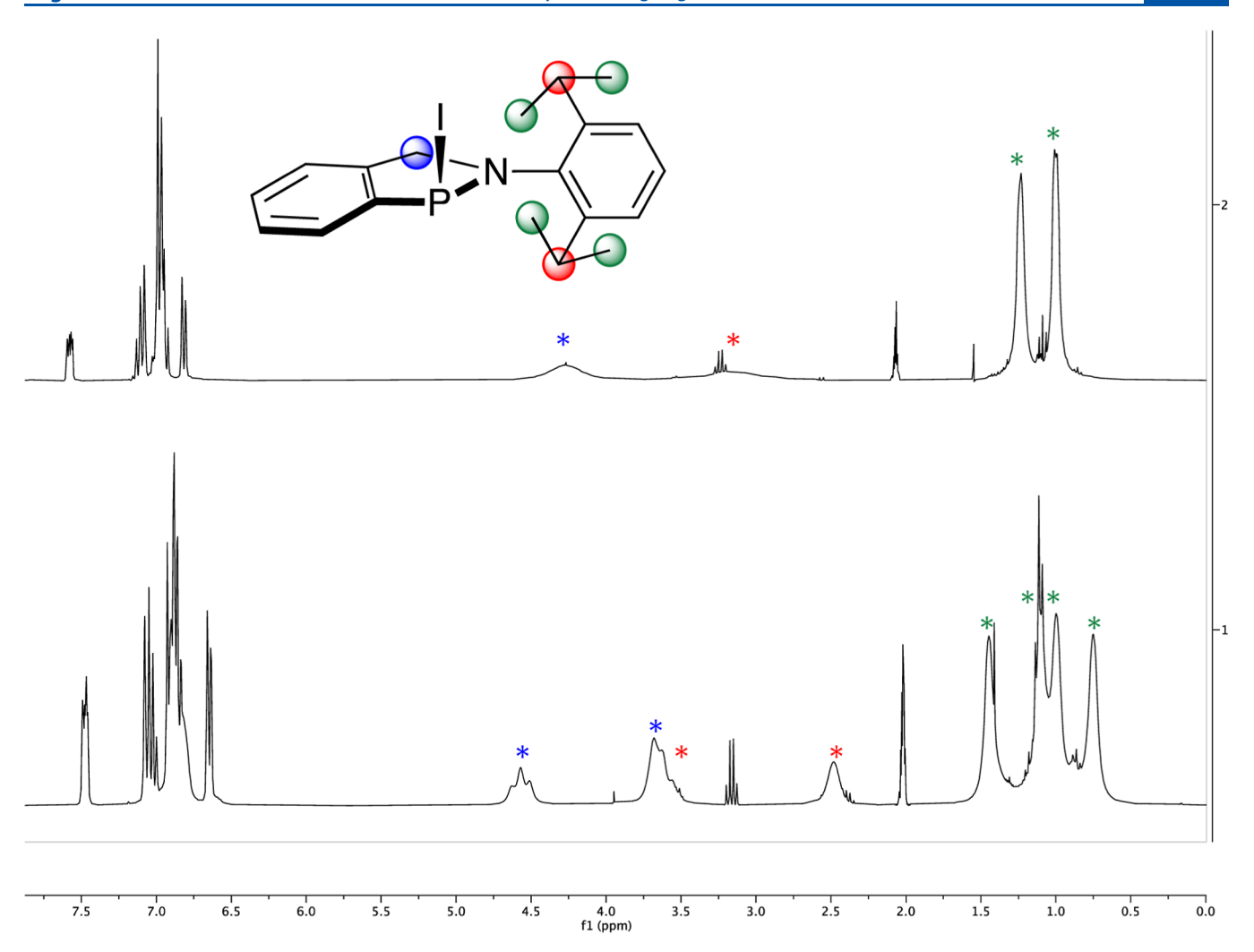


Figure 4. ¹H NMR spectrum (C₇D₈) of 1-I at room temperature (top) and -60 °C (bottom). Note: trace Et₂O signals at 1.10 and 3.25 ppm.

Table 1. DFT (B3LYP-D3/6-311G**++)-Calculated Barriers to P-Inversion (kcal/mol) in Compounds 1-X

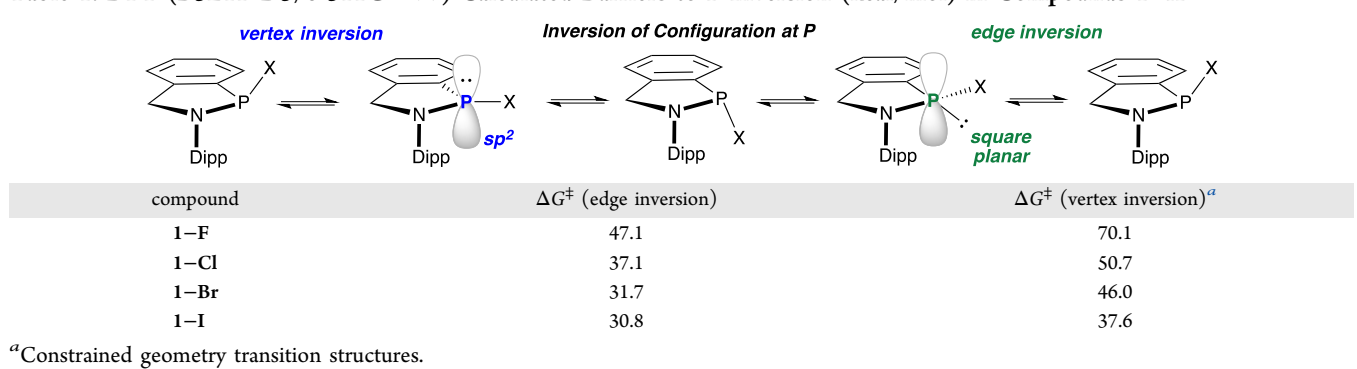


Table 2. DFT (B3LYP-D3/6-311 $G^{**}++$)-Calculated Homolytic and Heterolytic Bond Dissociation Free Energies (Gas-Phase; kcal/mol) for the P-X Bonds (X = Halogen) in Compounds 1

	P-X dissociation free energies (kcal/mol)		
compound	homolytic	heterolytic	
1-F	96.8	153.9	
1-Cl	63.2	114.7	
1-Br	48.9	120.1	
1-I	39.7	109.3	

loosely bound dimer lies only slightly higher in energy than 1-I and a more symmetrical transition structure that allows for I-transfer between phosphorus atoms lies only 18.5 kcal/mol above the monomer (bottom). Such a process is possible on the NMR timescale and would lead to inversion at each P, with the NMR site exchanges that are observed.

Such a bimolecular process requires a concentration-dependent rate of exchange. In agreement with the DFT prediction, the lineshapes of the ¹H NMR resonances in **1–I** were strongly dependent on concentration, as shown in Figure 6, with more concentrated samples showing sharper

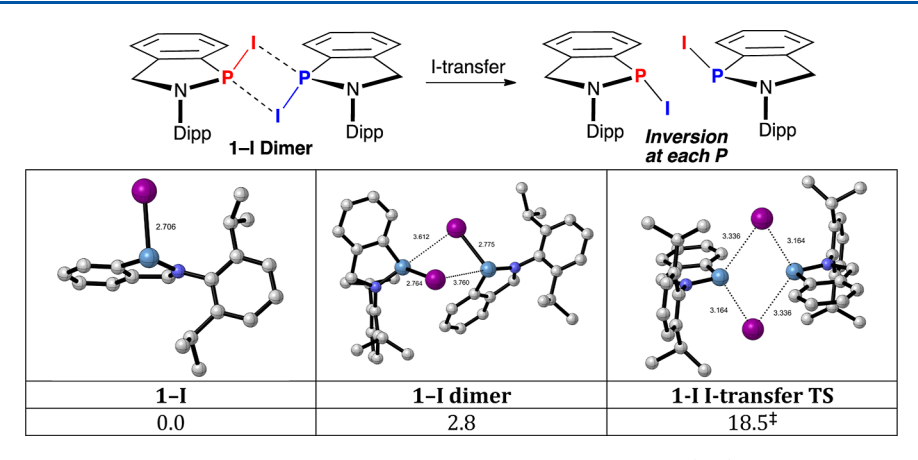


Figure 5. Schematic depicting the mechanism of biomolecular I-transfer leading to P-inversion (top) and DFT-calculated structures of 1–I, its weakly bound dimer, and a transition structure for I-transfer between P-atoms (bottom). Relative free energies are in kcal/mol.

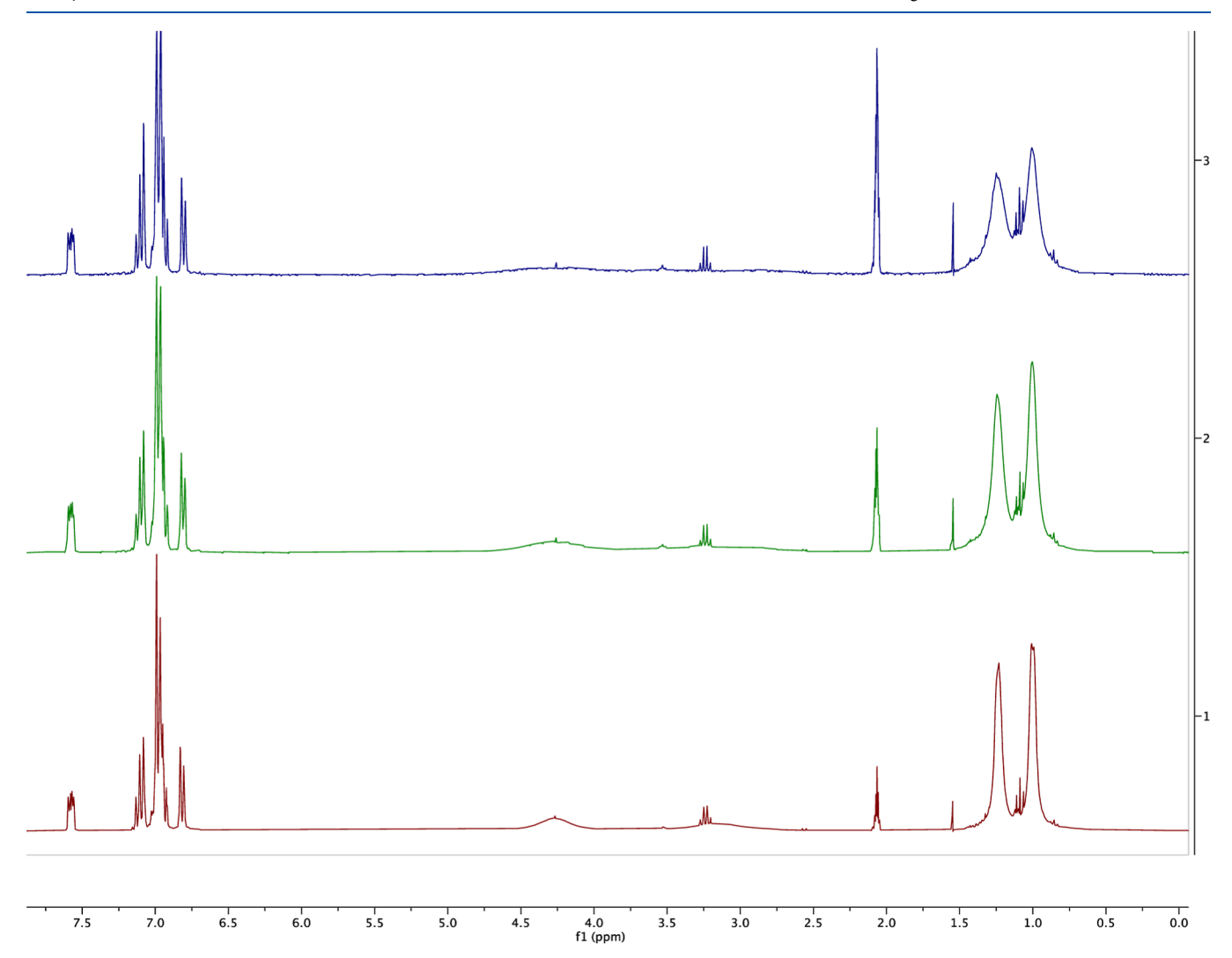


Figure 6. Effect of dilution on the ${}^{1}H$ NMR spectrum ($C_{7}D_{8}$) of 1–I at room temperature. The concentrated sample (bottom) is diluted by 2× (middle) and 4× (top) with progressive broadening of the lineshapes. Note: trace Et₂O signals at 1.10 and 3.25 ppm.

resonances due to increased rates of site exchange. While this bimolecular mechanism is initially surprising, weakly bound adducts of tertiary phosphines with the σ^* -holes of C–I bonds have recently been uncovered. The structures of these adducts similarly involve weak donation of the P_{LP} into the P–I antibonding MO of a second molecule, with the weak P–I

bond presumably facilitating I-transfer between phosphorus centers.

Unlike 1–I, no change in symmetry was observed by 1 H NMR spectroscopy between -60 and 80 $^{\circ}$ C for 1-Br and its structure was further corroborated by 13 C{ 1 H} NMR spectroscopy, with X-ray crystallography establishing that the C_{1}

symmetric structure was preserved in the solid state (Figure 7). This structure along with the other 1-X derivatives is

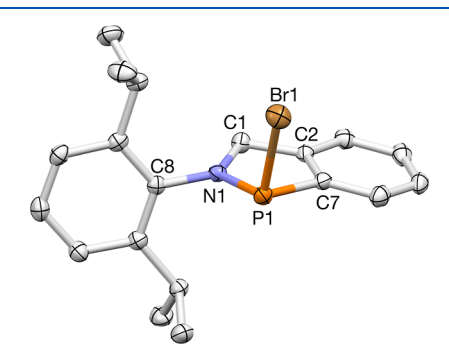


Figure 7. X-ray crystal structure of **1**–**Br**. Selected bond lengths (Å) and angles (°): P_1 – Br_1 = 2.3521(7), P_1 – N_1 = 1.661(2), P_1 – C_7 = 1.817(2), N_1 – C_1 = 1.476(3), N_1 – P_1 – Br_1 = 106.51(7), N_1 – P_1 – C_7 = 89.76(10), and C_7 – P_1 – Br_1 = 96.69(8).

compared with their NHP counterparts (3-X) in Table 3 (vide infra). Full details are provided in the Supporting Information.

To summarize, all P-halogenated benzazaphospholes (1) exhibit C_1 symmetry in the solid state, ¹⁸ and the ground-state C_1 geometry featuring a covalent P–X bond is maintained in solution.

Structures of P-Halogenated NHPs (3) and Comparison of Their Solid-State Structures to P-Halogenated Benzazaphospholes (1). While the pyramidal structures of 1-X are clearly established in the solid state and in solution, a comparison is warranted with their NHP analogues (3-X), in which phosphorus is flanked by an additional N lone pair. When N-(t-Bu)-substituted chloro NHP derivative 3-Cl was first prepared, 66,32 the molecule was described as ionic with an aromatic phosphenium cation with two planar N atoms and a chloride counterion. Solution properties such as deshielded ring protons observed by ¹H NMR spectroscopy, a downfield shifted ³¹P NMR resonance, and insolubility in hexanes and low volatility (in comparison with its saturated analogue) were presented as evidence in support of the ionic structure of 3-Cl. 6b Subsequent X-ray crystallographic analysis showed that the P–Cl bond was long [2.715(2) Å], but well within the sum of van der Waals' radii, leading to speculation whether "autoionization" was occurring in solution. 32 However, elongation of the P-Cl bond in 3-Cl could result instead from $N_{LP} \rightarrow \sigma^*(P-X)$ negative hyperconjugation (X = Cl, Scheme 3, right panel), an interaction invoked early on during an investigation into the conformation and stereodynamics of related P-NR₂-functionalized benzodiazaphospholes.³³ An intrinsic problem in using NMR spectroscopy to determine if the solution structures of P-halogenated NHPs are dissociated

is that the C_2N_2 backbone is constructed from symmetrical 1,4-diazadienes ^{16a} (or their closely related diazadiene dianions), ³² leading to a product (like 3–Cl) that has a mirror plane (C_s symmetry) whether or not the P–X bond is intact (Scheme 3, left panel).

If $N_{LP} \rightarrow \sigma^*(P-X)$ negative hyperconjugation is responsible, the extent of bond lengthening could be dependent on both the N-substituent and the polarizability of X⁻. An extensive X-ray crystallographic investigation of 3-Cl established that N-(t-Bu) and -Cy donors afforded exocyclic P-Cl bonds that could be elongated by more than 0.4 Å relative to P-halogenated NHPs featuring N-aryl groups like Mes (2,4,6trimethylbenzene) and Dipp,³⁴ consistent with the better electron-releasing properties of the alkyl substituents (Figure 8, left). A follow-up study using N-(t-Bu) analogues of the remaining members of the halogen series $(3-F \rightarrow 3-I)$ showed that the P-F bond featured minimal elongation $[1.6544(14) \text{ Å}],^{24}$ while the P-Br (2.947(1) Å) and P-I (3.426(1) Å) bonds were more significantly lengthened.²³ In particular, the P-I bond length in 3-I approached the sum of van der Waals radii (3.78 Å) and showed close intermolecular contacts in the solid state with the P-center (3.558(1) Å) of an adjacent C₂N₂P ring, leading to its formulation as an ionic species (Figure 8, right).²³

The X-ray crystallographic analysis also shows that the Natom of related P-halogenated benzazaphospholes 1-F through 1-I is planar (sp²); ¹⁸ therefore, their exocyclic P-X bonds are also susceptible to $N_{LP} \rightarrow \sigma^*(P-X)$ negative hyperconjugation. Previously, a DFT/NBO comparison of 1and 3-Cl with their corresponding P-CCPh derivatives indicated that the shorter P-X (X = Cl, CCPh) bonds observed in functionalized benzazaphospholes were a result of less-extensive N-lone pair delocalization into the P-X σ^* orbitals than the NHP analogues (one vs two nitrogen donors). With the halogen series of P-heterocycles 1 and 3 completed, additional comparisons can be made, as presented in Table 3. The P-F bonds in 1-F and 3-F are equal within error, 24,25 suggesting that the polarizability of the Xcomponent (or lack thereof in the case of F) plays a larger role than the number of nitrogen donors. In contrast, the P-X bonds in 3-Cl and 3-Br are more than 0.5 Å longer than their 1-Cl and 1-Br counterparts, while the difference in P-I bond lengths in 3–I versus 1–I is approaching 0.9 Å!^{23,24} It is worth noting that the halogen series in NHPs (3) has N-(t-Bu) substituents, which are known to maximize the length of the exocyclic P-X bond (vide supra, Figure 8, left), 34 while derivatives of 1 feature an N-Dipp group; however, even an N-Dipp analogue of 3-Cl (3-Cl*) had a longer P-Cl bond by almost 0.1 Å. It might be expected that if P-X bond elongation is due to $N_{LP} \rightarrow \sigma^*(P - \hat{X})$ negative hyperconjugation, the longer P-X bonds in compounds 3-Cl through 3-I should be accompanied by shorter P-N bonds, but all the P-N bonds in

Table 3. Selected P-X and P-N Bond Lengths in 1/3-F $\rightarrow 1/3$ -I in Comparison to Average P-X Bond Lengths (X = Halogen)^a

	1-F	3-F	1-Cl	3-Cl	3-Cl*	1-Br	3-Br	1-I	3-I
P-X bond	1.6569(15) Å	1.6544(14) Å	2.1649(8) Å	2.6915(4) Å	2.243(1) Å	2.3521(7) Å	2.947(1) Å	2.5937(7) Å	3.426(1) Å
P-N bond	1.6716(15) Å	1.672(2) Å 1.6721(19) Å	1.6681(16) Å	1.6628(8) Å 1.6651(8) Å	1.684(1) Å 1.679(1) Å	1.661(2) Å	1.657(2) Å 1.666(2) Å	1.6657(17) Å	1.663(2) Å 1.669(3) Å
average P–X bond	1.583 Å		~2.18 Å			$2.30 \pm 0.1 \text{ Å}$		2.45 Å	

^a3-CI* is an N-Dipp-substituted NHP.³⁴

Scheme 3. Ionic vs Covalent Structure of 3-Cl (Left) and Orbitals Involved in Negative Hyperconjugation in P-Heterocycles 3 and 1 (Right, Note: the N-Substituents Have Been Drawn as Methyl Groups for Simplicity)

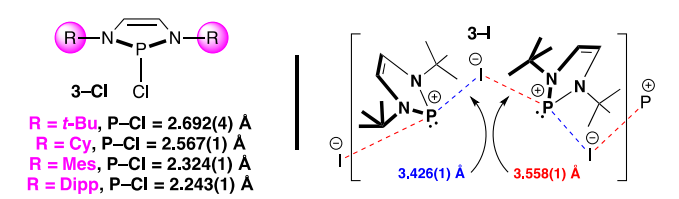


Figure 8. Effect of the *N*-substituent on P–Cl bond length in 3–Cl (left) and a depiction of the P–I contacts in the solid-state structure of 3–I (right).

derivatives of 1 and 3 are ~ 1.66 Å. Some previously reported average P–F, P–Cl, P–Br, and P–I bond lengths are shown in the bottom row of Table 3, highlighting how P-halogen bonds in derivative 1 are generally above average, while P–X bonds in NHP analogues 3 are unusually long. However, factors influencing bond distances in the solid state may also involve intermolecular interactions, such as those depicted in Figure 8 (right), which may amplify, distort, or otherwise conceal any intrinsic intramolecular factors that affect the bond distances.

Consequently, a DFT/NBO analysis was performed on the full molecules 1-X in the gas phase; results are presented in Table 4. Full details of the structures are provided in the Supporting Information. The DFT calculations reproduce satisfactorily the magnitudes and trends in P-X distances and the lack of variation of P-N distances, observed crystallographically for compounds 1-X. NBO data illustrate increasing depletion of the $N_{\rm LP}$ and increased occupancy of the P-X σ^* NBO, coupled with increasing negative hyperconjugative stabilization, on descending the halogen series. As expected, the P-X bond ionicities decrease as the halogen becomes heavier. These numbers are consistent with negative hyperconjugation being a significant contributor to P-X bond lengthening in these compounds and are inconsistent with ionization of the heavier halogens.

A more extensive study was made using smaller model compounds; the NMe analogues of 1-X ($\alpha-NMe$) and 3-X ($\alpha,\alpha'-NMe$) and an analogue with a flanking CH_2 group replacing NMe (in 1-X) to eliminate negative hyperconjugation from any N_{LP} . Results are shown in Table 5.

The structural and NBO data for the α -NMe derivatives are almost identical to that of the full molecule N-Dipp analogues (1–F through 1–I) in Table 4. Replacement of the α -NMe with CH₂ essentially eliminates the negative hyperconjugative occupancy of the P–X σ^* NBO, and in each case, the P–X bond length *decreases* relative to the α -NMe analogue. Doubling the number of flanking NMe groups (analogues of 3) results in increased negative hyperconjugation and *increased* P–X bond lengths, although nothing close to matching the unusually long P–I bonds observed in the solid state of 3–I. We conclude that any unusual long P–X distances observed crystallographically likely result from intermolecular interactions and are not necessarily reflective of any intrinsic intramolecular ionic character of these compounds.

Reactivity of P-Heterocycles 1–X with Pt(0). Heavier P-Halogenated Derivatives. Despite the shorter P–I bonds in the solid state relative to 3–I, 1–I can promote X-type ligand exchange via σ -bond metathesis³⁶ at Pd(II) centers and reacts with [Pd(P(t-Bu)₃)₂] to form an unusual Pd(I)–Pd(I) dimer (Scheme 4).¹⁸ Normally, these dimers are prepared via comproportionation between a Pd(0) and a Pd(II) source³⁷ and often feature symmetrical halogen bridges;^{38,39} however, here, the Pd(I) dimer is formed via a possible bimetallic oxidative addition⁴⁰ with an unprecedented Pd₂(μ–I)(μ–PN) core that is stabilized by bulky, terminal P(t-Bu)₃ donors and a Pd–Pd bond [2.6215(3) Å].¹⁸

Given its unique structure, we questioned if related and more robust complexes would be supported at a Pt center. Indeed, treatment of both **1**–**Br** and **1**–**I** with $[Pt(P(t-Bu)_3)_2]$ gave Pt(I)-Pt(I) dimers **4**–**Br** and **4**–**I**, respectively (Scheme 5). Their formation was readily identified by $^{31}P\{^1H\}$ NMR spectroscopy (see Figure 9 for 4–**I**), which displayed a diagnostic triplet/doublet pattern (**4**–**Br**: $J_{PP} = 129$ Hz and 4–**I**: $J_{PP} = 104.5$ Hz), integrating in a 1:2 ratio with the corresponding Pt satellites (**4**–**Br**: $^1J_{Pt-PN} = 5205$ Hz, $^1J_{Pt-P(t-Bu)_3} = 5414$ Hz; **4**–**I**: $^1J_{Pt-PN} = 4774$ Hz, and $^1J_{Pt-P(t-Bu)_3} = 5374$ Hz).

The upfield signal in 4–I (δ 109) featured further splitting due to the presence of the isotopologue with a single ¹⁹⁵Pt atom (see the inset of Figure 9), which renders the P(t-Bu) $_3$ donors spectroscopical inequivalence; one terminal phosphine

Table 4. DFT-Calculated Distances, NBO Occupancies, Bond Ionicities, and $N_{LP} \rightarrow P - X(\sigma^*)$ Delocalization Energies (kcal/mol) for the P-X Bonds in Compounds 1-X

	distances (Å) NB		NBO oc	cupancy (e)			natural charges	
compound	P-X	P-N	N_{LP}	Р-Х σ*	$N_{LP} \rightarrow P - X(\sigma^*)$ delocalization (kcal/mol)	P	X	P-X % ionicity
1-F	1.690	1.692	1.80	0.14	18.5	1.28	-0.60	66
1-Cl	2.222	1.690	1.78	0.18	21.9	1.06	-0.41	45
1-Br	2.491	1.686	1.76	0.23	28.4	1.03	-0.39	41
1-I	2.706	1.688	1.76	0.23	27.9	0.96	-0.32	33

Table 5. DFT-Calculated Distances, NBO Occupancies, Bond Ionicities, and $N_{LP} \rightarrow P-X(\sigma^*)$ Delocalization Energies (kcal/mol) for the P-X Bonds in Analogues of Compounds 1 and 3

α,α'-NMe-P-F	α,α'-NMe-P-Cl	α,α'-NMe-P-Br	α,α'-NMe-P-I
1.707	1.702 100.8 2.342	1.701	99.5 2.852
	NBO occupano	cy P–X σ*	
0.24	0.36	0.44	0.47
	NBO occupanc		
1.73	1.69	1.67	1.66
	2N _{LP} →P-X(σ*) Deloca	lization (kcal/mol)	
36.8	50.6	62.4	62.6
α-NMe-P-F	α-NMe-P-Cl	α-NMe-P-Br	α-NMe-P-I
1.690	1,892	1,687 103,3 2,484	1.690
	NBO occupano	cy P–X σ*	
0.15	0.18	0.22	0.23
1.50	NBO occupa	ncy N _{LP}	1.70
1.79	1.78	1.76	1.76
18.5	$1N_{LP} \rightarrow P - X(\sigma^*) \text{ Deloca}$ 20.5	1ization (kcal/mol) 26.0	26.0
18.5	40.5	20.0	40.0
α-CH ₂ -P-F	α-CH ₂ -P-Cl	α-CH ₂ -P-Br	α-CH ₂ -P-I
1.863 98.0 1.672	1.668 98.2 2.158	1.866 97.9 2.395	1.872 98.9 2.595
	NBO occupano		
0.06	0.06	0.08	0.08

Scheme 4. Previously Documented Reactivity between 1–I and Pd Complexes¹⁸

$$[Pd(P(t-Bu)_3)_2]$$

$$(t-Bu)_3P - Pd - P(t-Bu)_3$$

$$(t-Bu)_3P - Pd - Pd - P(t-Bu)_3$$

$$Ar = p-XC_6H_4$$

$$X = Me \text{ or } F$$

$$+ trans-Pdl_2(PEt_3)_2$$

is directly bound to the NMR-active ¹⁹⁵Pt nucleus, while the other is not. Therefore, two sets of satellites are generated. ⁴² The outer set is derived from one-bond Pt-P coupling $\binom{1}{J_{\text{Pt-P}}}$

= 5374 Hz), resonating as a doublet of doublets of doublets $(^2J_{PP} = 104.5 \text{ Hz and } ^3J_{PP} = 57 \text{ Hz})$. The expected eight-line pattern of the inner set partially overlaps with central doublet at 109 ppm, but the two-bond Pt-P coupling can be extracted $(^2J_{Pt-P}=41 \text{ Hz})$ along with the matching $^2J_{PP}$ and $^3J_{PP}$ coupling constants. Using MestreNova, 43 simulated 31P NMR signals of 4-I that closely fit the experimental spectrum were produced and are shown in Figure 9. Additional ³¹P NMR signals due to the doubly labeled isotopologue (two ¹⁹⁵Pt nuclei), which have been previously observed in related Pt(I)-Pt(I) dimers 42,44 and should statistically compose approximately one-ninth of the product, were not observed, even on the 600 MHz NMR spectrometer (242 MHz for ³¹P nuclei). Although featuring slightly different ${}^{1}J_{Pt-P}$, ${}^{2}J_{PP}$, and ${}^{3}J_{PP}$ values, the ${}^{31}P\{{}^{1}H\}$ NMR spectrum of 4-Br mirrored what was observed with 4-I. Although, in this case, the inner set of satellites was more obscured by the central doublet (δ 102) and the ${}^2I_{\text{Pt-P}}$ coupling constants could not be determined and the ${}^{3}J_{PP}$ coupling constant could not be corroborated with the outer satellites (${}^{3}J_{PP}$ = 50.5 Hz). However, this ${}^{31}P\{{}^{1}H\}$ NMR

Scheme 5. Synthesis of 4-Br/I

spectrum was also simulated with MestreNova and is shown in the Supporting Information.

Fortunately, the 1 H NMR spectra of 4–Br/I were much simpler, featuring a single signal for the benzylic CH $_2$ protons and a sole methine resonance, indicative of the presence of a mirror plane. The expected two doublets for the two independent methyl groups of the locked N-Dipp substituent are present in the alkyl region but are partially overlapped/underneath the prominent doublet of the $P(t\text{-Bu})_3$ donors. $^{13}\text{C}\{^1\text{H}\}$ NMR spectroscopy further corroborated the structural assignment as 10 aryl, 5 alkyl, and a benzylic signal were observed. Ultimately, X-ray crystallography and elemental analysis established the solid-state structure and bulk purity of 4-Br/I (Figures 10 and 11).

The solid-state structures of 4-Br/I are reminiscent of a well-known class of Pt(I)-Pt(I) dimers (5) (Figure 12 for structure), which feature terminal phosphine (5a)⁴⁵ or phosphinite (5b)⁴⁶ donors with the same bridging phosphido groups (μ -PR₂, R = Ph or Cy) that are further supported by a Pt-Pt bond of approximately 2.6 Å.47 However, the substitution of one of the μ -PR₂ units for a halide (μ -X, X = Br or I) does introduce some differences, including a four-atom core $[Pt_2(P)(X), P = bridging P-heterocycle]$ without D_{2h} symmetry⁴⁸ containing long Pt-X bonds and an acute Pt-X-Pt bond angle.⁴⁷ In addition, unlike 5, the Pt-P bond lengths to the bridging phosphido in 4-Br/I are shorter than those to the terminal phosphine, which is likely a consequence of the small steric profile of a nearly planarized (one sp³-hybridized benzylic carbon) P-heterocycle in combination with an elongated bond to the bulky $P(t-Bu)_3$ ligands. The table embedded in Figure 12 emphasizes that these structural differences are subtle as the Pt-Pt, Pt-phosphido, and Ptphosphine bond lengths in 4-Br/I and 5a/b are nearly identical.45-47

The remarkable difference between 4-Br/I and 5a/b is in their methods of preparation. Dimer 5a is the product of thermal decomposition of Pt(PPh₃)₄ in benzene, 45 while **5b** is generated from cis-PtCl₂(PHCy₂) and excess NaOMe. 46 Other Pt(I)-Pt(I) complexes with neutral terminal phosphine donors (and in some cases, isocyanates) and bridging phosphide ligands have been synthesized by treatment of Pt(II) monomers of the type $PtX_2(PRR_2)_2(X = halide, R = H$ or alkyl, and R' = alkyl) with strong nucleophiles [LiP-(SiMe₃)₂] or sodium metal⁴⁷ or from Pt(II) dimers like $[PtH(PH(t-Bu)_2)(\mu-P(t-Bu)_2)]_2$ via a two-step "oxidantinduced hydride abstraction"/deprotonation sequence. 49 Here, the addition of 1-Br/I to the Pt(0) source Pt(P(t-I)) $Bu)_3$ affords Pt(I)-Pt(I) dimers 4-Br/I, a transformation resembling bimetallic oxidative addition.⁵⁰ However, as observed with binuclear Pd(II) paddlewheel complexes⁵¹ and related analogues and Au(I)-Au(I) bis(phosphorus-ylide) derivatives, 52 bimetallic oxidative addition normally involves two metal centers that are prelinked by a bridging ligand, with

the redox event resulting in an increase in the oxidation state of each metal by one and the formation of a M–M bond.⁴⁰

The mechanism of formation of 4-Br/I must follow a different pathway and was probed using DFT calculations at the B3LYP-D3/LACV3P**++ level; this method and basis set give very good agreement with the metrics of those starting materials and products characterized by X-ray crystallography. Since the reactions occur in nonpolar media, a solvent correction was not used. Several pathways were considered, starting with the two-coordinate $Pt(P^tBu_3)_2$ complex starting material and affording the structures shown in Scheme 6. Direct dissociation of PtBu3 to give the monocoordinate Pt(P^tBu₃) as a reactive species is uphill by almost 40 kcal/mol and is unlikely to play a role in the reaction. Binding of 1-X to $Pt(P^tBu_3)_2$ to give three-coordinate intermediate A-X is also uphill, presumably due to contraction of the angle between extremely bulky P^tBu₃ ligands. Transition structures for P-X oxidative addition evolving from these three coordinate intermediates A-X must be even more strongly uphill due to the decreasing angle between PtBu3 ligands in the "tetrahedral" or "cis square-planar" pathways shown and could not be located. Attempts to locate the illustrated "tetrahedral" or "cis-square-planar" intermediates that would result from these oxidative addition pathways led only to in silico ligand dissociation.

However, loss of P^tBu₃ from A-X is downhill to give two coordinate B-X intermediates, from which P-X oxidative addition can occur to give a T-shaped intermediate C-X. This reaction is downhill from B-X, with low-energy transition structures B-X (TS) for X = Br and I, slightly uphill from B-IX with a higher-energy transition structure for X = Cl, and strongly uphill for X = F; the transition structure for oxidative addition of P-F could not be located. The facility of oxidative addition reflects the relative strengths of the P-X bonds and the resultant Pt-X bonds. Finally, intermediate C-X can be trapped by $Pt(P^tBu_3)_2$ to give a transient species **D**-**X** from which dissociation of P^tBu₃ is facile to afford the final observed products 4-X. Attempts in silico to coordinate additional $P^{t}Bu_{3}$ to 4-X (X = I, Br, and Cl) to afford D-X resulted in dissociation of the added ligand. Undoubtedly, the formation of dimers 4-Br/I via this two-coordinate pathway is favorable with very bulky ligands (P^tBu₃), but other options for P-X bond activation from a three-coordinate intermediate may be possible with less-hindered Pt systems.

Lighter P-Halogenated Derivatives. As predicted by DFT, oxidative addition of P–Cl and P–F bonds to two-coordinate B–X intermediates (see Scheme 6) involves less-accessible high-energy transition structures. Indeed, treatment of 1-F/Cl with $[Pt(P(t-Bu)_3)_2]$ generated unidentified product mixtures with their $^{31}P\{^1H\}$ NMR spectra characterized by ill-defined and broad peaks lacking any diagnostic Pt satellites. However, other Pt(0) sources with smaller phosphine ligands may open alternative pathways of P–Cl or P–F bond activation (vide

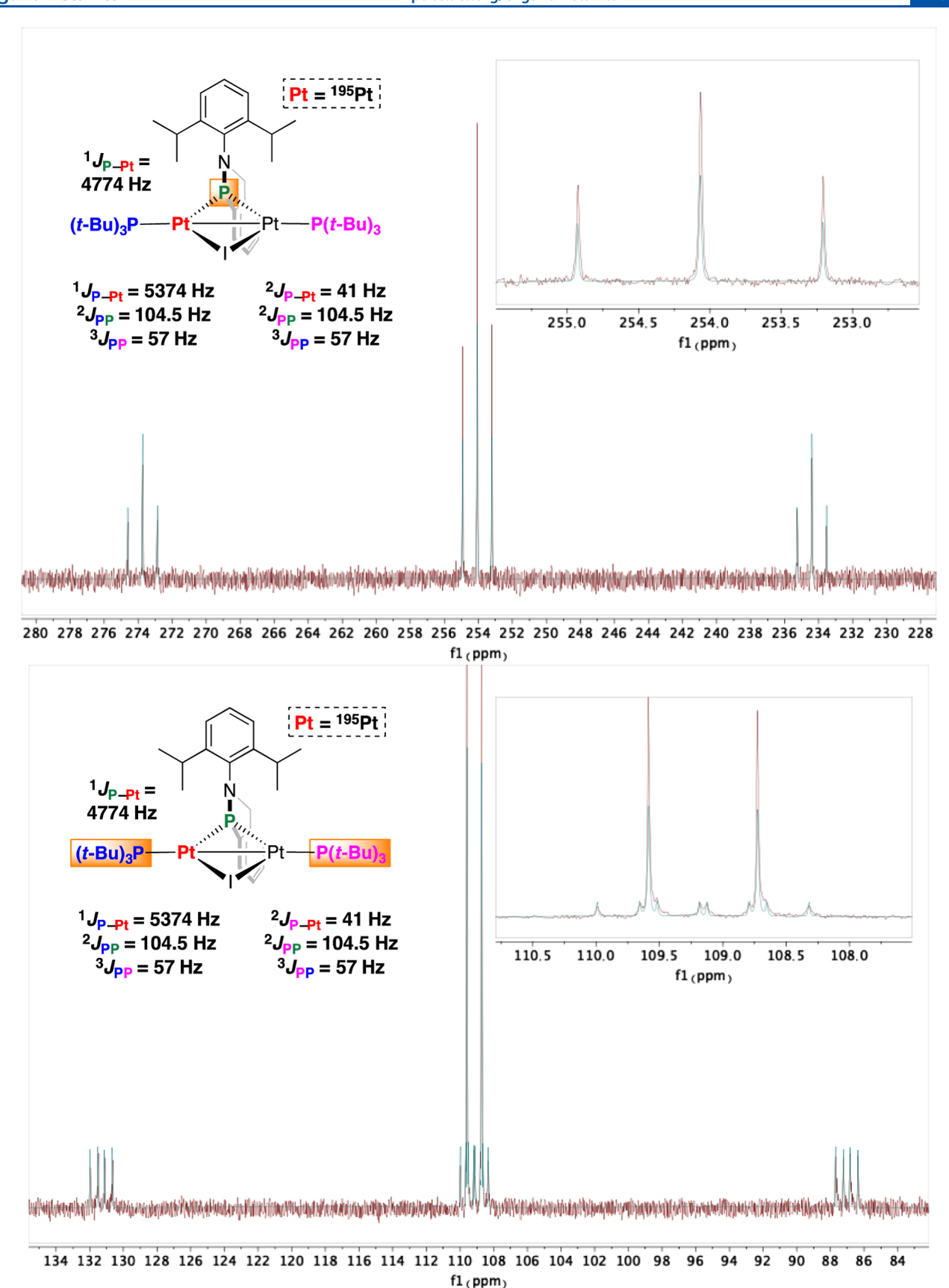


Figure 9. Experimental (red) and simulated (blue) NMR spectra with ³¹P signals at 254.0 (top) and 109.1 (bottom) ppm for the two most abundant isotopologues of 4–I at 121.38 MHz. The upper-right insets show the match of the central pattern for each ³¹P signal, while the ChemDraw insets (upper left) identify the specific P-donor(s) responsible for the signal (orange box) and the corresponding *J* values.

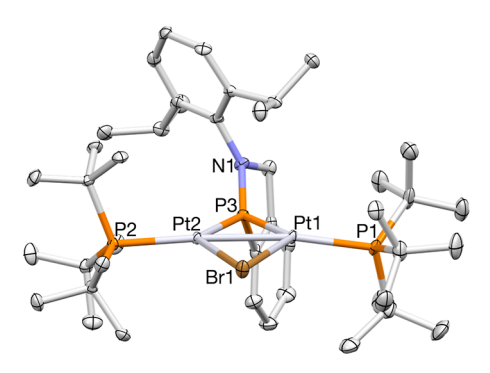


Figure 10. X-ray crystal structure of **4–Br**. Selected bond lengths (Å) and angles (°): $Pt_1-Pt_2=2.6000(2)$, $Pt_1-P_1=2.2722(11)$, $Pt_1-P_3=2.2340(10)$, $Pt_2-P_2=2.2864(10)$, $Pt_2-P_3=2.1968(10)$, $Pt_1-Br_1=2.6524(4)$, $Pt_2-Br_1=2.5900(4)$, $Pt_2-P_3-Pt_1=71.86(3)$, and $Pt_2-Br_1-Pt_1=59.450(9)$.

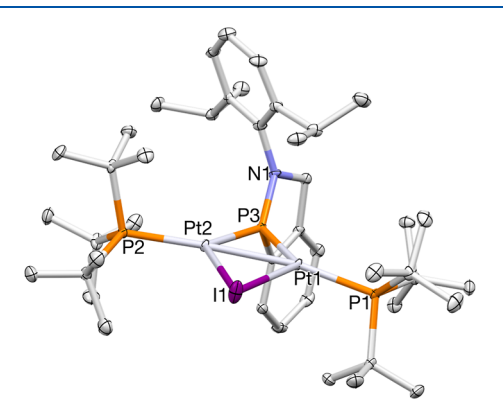


Figure 11. X-ray crystal structure of 4–I. Selected bond lengths (Å) and angles (°): $Pt_1-Pt_2=2.6219(2)$, $Pt_1-P_1=2.2826(10)$, $Pt_1-P_3=2.2400(10)$, $Pt_2-P_2=2.2925(10)$, $Pt_2-P_3=2.2126(10)$, $Pt_1-I_1=2.7220(3)$, $Pt_2-I_1=2.6890(3)$, $Pt_2-P_3-P_1=72.15(3)$, and $Pt_2-I_1-Pt_1=57.961(7)$.

supra). To test this, 1–F was added to Pt(PPh₃)₄, resulting in conversion to a major product, formulated as [Pt(1–F)(PPh₃)₂] (6) featuring a doublet of triplets centered at 183.6 ppm (${}^{1}J_{\text{PF}} = 1060 \text{ Hz}$ and ${}^{2}J_{\text{PP}} = 205 \text{ Hz}$) and a doublet of doublets at 49.7 ppm (${}^{2}J_{\text{PP}} = 205 \text{ Hz}$, ${}^{3}J_{\text{PF}} = 48 \text{ Hz}$) with the corresponding Pt satellites (${}^{1}J_{\text{Pt-PN}} = 6550 \text{ Hz}$ and ${}^{1}J_{\text{Pt-PPh}_3} = 4232 \text{ Hz}$), integrating in a 1:2 ratio as determined by ${}^{31}P\{{}^{1}H\}$ NMR spectroscopy (Scheme 7).

The increase in the ${}^{1}J_{PF}$ coupling constant (relative to 1-F) of the downfield signal (δ 183.6) confirmed that the strong P– F bond⁵³ was not cleaved and rehybridization of the P-center to ~sp3 occurred. Furthermore, the presence of a strained fivemembered P-containing ring and a highly electronegative Fsubstituent leaves the P-lone pair with a substantial amount of s-character,⁵⁴ which is reflected in the large ¹J_{Pt-P} coupling constant; related homoleptic Pt(0) complex Pt(PF₃)₄ features a comparable ${}^{1}J_{Pt-P}$ value (6480 Hz). The smaller ${}^{1}J_{Pt-P}$ coupling constant of the upfield PPh3 resonance is indicative of less s-character in the Pt-P bond with ³J_{PF} values in the same range as Pt(triphos)L complexes [triphos = CH₃C- $(CH_2PPh_2)_3$, L = PF₃, PF₂(OPh), and PF₂NMe₂, $J \sim 47$ Hz].⁵⁵ Unfortunately, isolation of **6** was problematic likely due to the combination of a labile Pt(0) center, a weakly basic (high s character) P-heterocycle derived ligand, and free and exchanging PPh3 in solution. Recrystallization of 6 from hot acetonitrile deposited X-ray quality crystals of 7 (Figure 13). Pt(0) complex 7 contains 1-F and PPh₃ donors in a 2:1 stoichiometry, the opposite of what was detected with 6 in solution by ³¹P{¹H} NMR spectroscopy (vide supra), reflecting that ligand exchange, especially in a coordinating solvent (like CH₃CN), is a low barrier process in these d¹⁰ metal systems.

Like 1-F, if 1-Cl prefers to coordinate to Pt(0) centers supported by less-bulky phosphine donors through its P-lone pair without P-X bond scission, these complexes may also be especially labile. Indeed, addition of 1-Cl to Pt(PPh₃)₄ and $Pt(PPh_3)_2(C_2H_4)$ in toluene, tetrahydrofuran (THF), or dichloromethane (DCM) consumed the starting materials but generated product mixtures analyzed by ³¹P{¹H} NMR spectroscopy that possess unidentifiable and/or broadened peaks without Pt-satellites. Only reactions conducted between 1-Cl and $Pt(PPh_3)_4$ or $Pt(PPh_3)_2(C_2H_4)$ in acetone resulted in sharp 31P NMR signals of the same unidentified Ptcontaining product, which featured two doublets with a large $J_{\rm PP}$ coupling (509 Hz) at 110 ($J_{\rm Pt-P}$ = 4047 Hz) and 30.5 ($J_{\rm Pt-P}$ = 2811 Hz) ppm. This NMR spectroscopic data suggests two distinct P-donors, one likely derived from the heterocyclic unit of 1-Cl and the other from PPh3, that are now connected by a P-P bond and coordinated to Pt, affording an unisolable PtP₂ metallacyclopropane structural unit tentatively assigned as 8 (Scheme 8, left panel). Related three-membered rings of WP₂and RhP₂-type complexes have similarly large PP coupling constants (right panel). ^{56,57} Other well-defined ³¹P NMR

	4-Br	4-I	5a	5b
Pt-Pt bond	2.6000(2) Å	2.6219(2) Å	2.604(1) Å	2.6307(5) Å
Pt-Phosphine	2.2722(11) Å	2.2826(10) Å	2.218 Å	2.2150(14) Å
bond	2.2864(10) Å	2.2925(10) Å	2.246 Å	
Pt-Phosphido	2.1968(10) Å	2.2126(10) Å	2.300, 2.324,	2.3058(14) Å
bond	2.2340(10) Å	2.2400(10) Å	2.317, and	
			2.307 Å	
Pt-X bond	2.5900(4) Å	2.7220(3) Å	N/A	N/A
(X = Halogen)	2.6524(4) Å	2.6890(3) Å		

Figure 12. Structures and selected bond lengths in 4-Br/I and 5a/b.

Scheme 6. DFT-Calculated Pathways for Oxidative Addition of P-Halogen Bonds to Pt(0) via Two- and Three-Coordinate Intermediates^a

^aRelative free energies are given in kcal/mol.

Scheme 7. Synthesis of 6

resonances from the crude reaction include singlets observed at 122, 24, and 18 ppm. Recrystallization of these product mixtures at -35 °C precipitated X-ray quality crystals of *trans*-Pt(PPh₃)₂(H)(Cl),⁵⁸ a Pt(II) complex likely derived from oxidative addition between a Pt(PPh₃)₂ fragment and HCl.⁵⁹

Both the formation of a structural unit like 8 and *trans*-Pt(PPh₃)₂(H)(Cl) could result from heterolytic P–Cl bond cleavage of 1–Cl in acetone at an electron-rich Pt(0) center. Previously, when a derivative of 3–Cl was exposed to W(0)⁶⁰ and *N*-Mes-substituted 3–Br was added to Pd(PPh₃)₄, a phosphenium donor was generated at the transition-metal center. Here, the related phosphenium ligand derived from 1–Cl could lose a proton from its benzylic carbon atom, liberating HCl into solution that reacts with a Pt(PPh₃)₂

intermediate to give *trans*-Pt(PPh₃)₂(H)(Cl) and 10π -electron benzazaphosphole **2** (Scheme 9, top pathway). In an analogous case, ⁶² treatment of Pt(IMes)₂ [IMes = 1,3-di(2,4,6-trimethylphenyl)imidazoline-2-ylidene, an NHC] with a boracyclohexadiene containing a B–Cl unit and an adjacent sp³-hybridized carbon center resulted in the synthesis of *trans*-Pt(IMes)₂(H)(Cl) and expulsion of a 6π -electron borabenzene. This mechanistic scenario is largely speculative even though as varying quantities of **2** (δ 182) and no phosphenium-type donors (δ > 200)² have been observed in the reaction mixtures by 31 P{ 1 H} NMR spectroscopy. However, any phosphenium produced is likely transient because they serve as excellent precursors to phosphametalacycles like the W(II) complex⁵⁶ shown in Scheme 8. In this

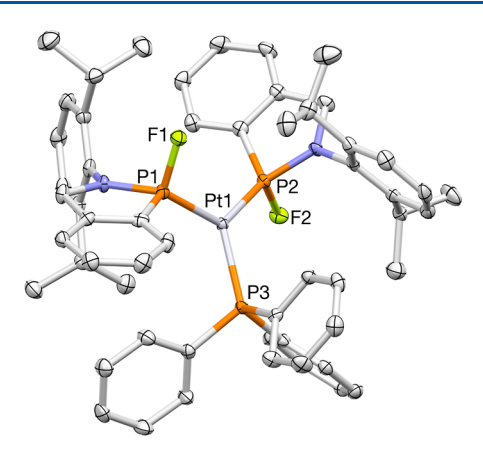


Figure 13. X-ray crystal structure of 7. Selected bond lengths (Å) and angles (deg): $Pt_1-P_1=2.2145(8)$, $Pt_1-P_2=2.2162(8)$, $Pt_1-P_3=2.2945(8)$, $P_1-F_1=1.618(2)$, $P_2-F_2=1.6265(19)$, $P_1-Pt_1-P_2=124.20(3)$, $P_1-Pt_1-P_3=115.76(3)$, and $P_2-Pt_1-P_3=120.00(3)$.

example, in order to construct a structural unit like **8**, one of the P–Ph units of a PPh₃ ligand must be cleaved, affording a phosphido (PPh₂⁻) that will trigger P–P bond formation with the cationic phosphenium (Scheme 9, bottom pathway). At this time, no spectroscopic evidence for the required P–C bond cleavage event like the formation or oxidative addition of chlorobenzene (PhCl) has been discovered.⁶³

The reactivity of 1-F through 1-I with Pt(0) sources is linked to the decreasing strength of the P-X bonds^{23,41} descending down the halogen series. Heavier halogenated analogues 1-Br and 1-I underwent an unusual bimetallic oxidative addition-type reaction with $[Pt(P(t-Bu)_3)_2]$, affording Pt(I)-Pt(I) dimers 4-Br and 4-I with a Pt₂(μ -I)(μ -PN) core that is stabilized by bulky, terminal $P(t-Bu)_3$ donors and a Pt-Pt bond. DFT calculations revealed that oxidative addition proceeds from a two-coordinate $Pt(P(t-Bu)_3)(1-Br/I)$ intermediate to give a T-shaped complex, which is trapped by a second equivalent of $[Pt(P(t-Bu)_3)_2]$, followed by loss of $P(t-Bu)_3$, leading to product formation (4-Br/I). On the other hand, the lighter halogenated derivatives 1-F and 1-Cl were more resistant to P–X bond cleavage. 53,60 For example, treatment of Pt(PPh₃)₄ with 1-F resulted in Pt(0) complex 6 featuring two PPh3 ligands with a single heterocyclic P-donor bound through its lone pair with an intact P-F bond. During the recrystallization process, ligand scrambling occurred, furnishing X-ray quality crystals of Pt(1-F)₂(PPh₃) (7). ³¹P{¹H} NMR spectroscopy indicated that addition of 1-Cl to Pt(0) sources gave crude reaction mixtures and labile d10 metal complexes were generated. A static Pt-containing complex was formed only when 1-Cl was exposed to $Pt(PPh_3)_4$ or $Pt(PPh_3)_2(C_2H_4)$ in acetone, which we speculate may have a unique, but unverified PtP_2 structure like 8.

CONCLUSIONS

The synthesis and structural characterization of the entire series of P-halogenated benzazaphospholes 1 was completed. As determined by ¹H and ¹³C{¹H} NMR spectroscopy, 1-F, 1–Cl, and 1–Br are C_1 -symmetric in solution, while 1–I has effective C_s symmetry due to a rapid, concentration-dependent, inversion at phosphorus, shown by DFT calculations to involve a dimeric iodine-bridged transition structure. In contrast, all of these P-heterocycles have C_1 symmetry in the solid state with elongation of the P-X bonds as shown by DFT/NBO studies to involve increasing $N_{LP} \rightarrow \sigma^*(P-X)$ negative hyperconjugation down the halogen series. Exposure of 1-Br/I to $[Pt(P(t-Bu)_3)_2]$ afforded Pt(I)-Pt(I) dimers 4-Br/I in which the P-X bond was oxidatively added to the Pt center; the lighter analogues (1-F/Cl) were less susceptible to related cleavage of their P-halogen bonds. For example, treatment of 1-F with Pt(PPh₃)₄ gave Pt(0) coordination complex 6 featuring the P-heterocyclic ligand bound through its lone pair and two PPh3 ligands. Recrystallization attempts furnished Pt(0) complex 7, likely the result of facile ligand exchange in the d¹⁰ metal system as the 1-F and PPh₃ donors were now present in a 2:1 ratio. The addition of 1-Cl to Pt(PPh₃)₄ or $Pt(PPh_3)_2(C_2H_4)$ in acetone produced a static Pt-containing complex that was not isolated but may have a PtP2 metallacyclopropane structural unit like 8. Future studies will focus on generating phosphenium ions from P-heterocycles 1-X (see Scheme 1) and testing their reactivity toward small molecules.

EXPERIMENTAL SECTION

General Experimental Details. Unless otherwise specified, all reactions and manipulations were performed under a nitrogen atmosphere in a Vacuum Atmospheres GENESIS glovebox or using standard Schlenk techniques. All glassware was oven-dried overnight (at minimum) at 140 °C prior to use. Anhydrous solvents were purchased directly from chemical suppliers (Aldrich or Acros), pumped directly into the glove box, and stored over oven-activated 4 or 5 Å molecular sieves (Aldrich). 4 N HCl in dioxane, CsF, TMSCF₃, TMSBr, TMSI, [Pt(P(t-Bu)₃)₂], Pt(PPh₃)₄, and Pt-(PPh₃)₂(C₂H₄) were obtained from chemical suppliers (Strem, TCI, Aldrich, and Acros). Benzazaphosphole 2 was prepared by literature methods.²² NMR spectra were obtained on either Varian spectrometers operating at 300, 400, or 500 MHz or a Bruker 600 MHz spectrometer; all spectra are displayed in the Supporting Information. NMR chemical shifts are reported as parts per mllion relative to TMS and are referenced to the residual proton or ¹³C signal of the solvent (1 H CDCl₃, 7.27 ppm; 1 H C₆D₆, 7.16 ppm; 13 C CDCl₃, 77.16 ppm; and 13 C C₆D₆, 128.06 ppm).

Scheme 8. Generation of Tentatively Assigned Structural Unit 8 (Left Panel) and Related MP₂ Transition-Metal Complexes with Large PP Coupling Constants (Right Panel)^{56,57}

Scheme 9. Potential Mechanistic Pathways for the Formation of trans-Pt(PPh₃)₂(H)(Cl) (Top Pathway) and Tentatively Assigned PtP₂ Metalacyclopropane 8 (Bottom Pathway)

Synthesis of 1–F. Compound **2** (500 mg, 1.69 mmol) was dissolved in 10 mL of toluene in a 100 mL Schlenk flask with a screwtop Teflon cap. The Schlenk flask was taken out of the glovebox, placed under positive N₂ pressure, fitted with a rubber septum, injected with 4 N HCl (846 μ L, 3.38 mmol, 2 equiv.), and stirred for 30 min. The reaction mixture was placed back in the glovebox and concentrated in vacuo. The yellow residue was dissolved in THF (5 mL) and treated with a premixed (10 min) solution of CsF (257 mg, 1.69 mmol) and TMSCF₃ (500 μ L, 3.38 mmol, 2 equiv) in 5 mL of THF, and the reaction mixture was stirred overnight (~16 h). The heterogeneous solution was concentrated in vacuo, and the crude solid was extracted with pentane (3 × 5 mL) and filtered through a silica plug. The filtrate was concentrated to 10 mL and placed at -35 °C, yielding a white crystalline solid suitable for X-ray diffraction (283 mg, 0.898 mmol, 53%).

Anal. Calcd for $C_{19}H_{23}FNP$: C, 72.36; H, 7.35; N, 4.44. Found: C, 72.42; H, 7.53; N, 4.37. $^{31}P\{^{1}H\}$ NMR (202 MHz, $C_{6}D_{6}$): δ 150.1 (d, J = 1035 Hz). ^{19}F NMR (282 MHz, $C_{6}D_{6}$): δ -81.0 (ddd, J = 1035, 28, and 19 Hz). ^{1}H NMR (500 MHz, $C_{6}D_{6}$): δ 7.66 (m, 1H, Ar), 7.21 (m, 1H, Ar), 7.14–7.03 (m, 4H, Ar), 6.96 (m, 1H, Ar), 4.83 (ddd, J = 28 Hz, 16 Hz, and 5 Hz, 1H, CH₂), 4.17 (ddd, J = 19 Hz, 16 Hz, and 13.5 Hz, 1H, CH₂) 3.65 (septet, J = 7 Hz, 1H, CH) 2.81 (septet, J = 7 Hz, 1H, CH), 1.34 (d, J = 7 Hz, 3H, Me), 1.20 (d, J = 7 Hz, 3H, Me), 1.14 (d, J = 7 Hz, 3H, Me), 0.97 (d, J = 7 Hz, 3H, Me). $^{13}C\{^{1}H\}$ NMR (151 MHz, CDCl₃): δ 149.1 (Ar), 147.4 (Ar), 144.6 (Ar), 142.2 (apparent t, J = 12 Hz, Ar), 137.9 (d, J = 15 Hz, Ar), 130.4 (Ar), 129.0 (d, J = 28 Hz, Ar), 128.0 (Ar), 127.6 (d, J = 8 Hz, Ar), 124.1(Ar), 124.0 (Ar), 122.4 (Ar), 64.1 (dd, J = 14 and 7 Hz, CH₂), 28.2 (CH), 28.1 (CH), 25.1 (Me), 25.0 (d, J = 5 Hz, Me), 24.7 (Me), 24.5 (Me).

Synthesis of 1-Br. Compound 2 (250 mg, 0.846 mmol) was dissolved in 5 mL of toluene in a 100 mL Schlenk flask with a screwtop Teflon cap. The Schlenk flask was taken out of the glovebox, placed under positive N2 pressure, fitted with a rubber septum, injected with 4 N HCl (846 μ L, 3.38 mmol, 2 equiv.), and stirred for 30 min. The reaction mixture was placed back in the glovebox and concentrated in vacuo. The residue was dissolved in DCM (5 mL) and TMSBr (123 µL, 0.931 mmol, 1.1 equiv) and was added dropwise, and the reaction mixture was stirred overnight (~16 h). The homogeneous reaction mixture was then concentrated in vacuo, and the crude solid was dissolved in a 1:1 mixture of THF and pentane (10 mL) and cooled to -35 °C, affording an analytically pure white crystalline solid (212 mg, 0.563 mol, 67%). Crystals suitable for X-ray diffraction were obtained from a second recrystallization from THF/pentane. VT ¹H NMR Spectroscopy (C₇D₈) was also conducted at 400 MHz from $-60~^{\circ}\text{C}$ to 80 $^{\circ}\text{C}$ in 10 $^{\circ}\text{C}$ intervals.

Anal. Calcd for $C_{19}H_{23}BrNP$: C, 60.65; H, 6.16; N, 3.72. Found: C, 60.75; H, 6.12; N, 3.59. $^{31}P\{^{1}H\}$ NMR (162 MHz, CDCl₃): δ 156.8. ^{1}H NMR (400 MHz, $C_{7}D_{8}$): δ 7.56 (m, 1H, Ar), 7.17–7.04 (m, 3H, Ar), 7.00–6.95 (m, 2H, Ar), 6.81 (m, 1H, Ar), 4.89 (apparent t, J = 17 Hz, 1H, CH₂), 3.98 (dd, J = 20 Hz, 17 Hz, 1H, CH₂), 3.76 (septet,

J = 7 Hz, 1H, CH), 2.64 (septet, J = 7 Hz, 1H, CH), 1.45 (d, J = 7 Hz, 3H, Me), 1.19 (d, J = 7 Hz, 3H, Me), 1.09 (d, J = 7 Hz, 3H, Me), 0.87 (d, J = 7 Hz, 3H, Me). 13 C{ 1 H} NMR (151 MHz, CDCl₃): δ 149.0 (Ar), 146.8 (Ar), 143.9 (Ar), 143.4 (d, J = 26 Hz, Ar), 136.4 (d, J = 12 Hz, Ar). 130.3 (Ar), 128.5 (Ar), 128.3 (Ar), 128.2 (d, J = 8 Hz, Ar), 124.7 (Ar), 124.3 (Ar), 122.3 (Ar), 64.6 (d, J = 17 Hz, CH₂), 28.6 (CH), 28.4 (CH), 25.3 (overlapping Me), 24.9 (Me), 24.7 (Me).

Synthesis of 4–I. Iodophosphine 1–I (30 mg, 0.071 mol) was dissolved in toluene (4 mL) and added to $[Pt(P(t-Bu)_3)_2]$ (94 mg, 0.156 mol) and stirred overnight (16 h). The dark red reaction mixture was concentrated in vacuo, and the residue was washed with MeCN (10 mL). The crude product was recrystallized from a 1:1 mixture of toluene/MeCN (\sim 3 mL) at \sim 35 °C, affording X-ray-quality red crystals (33 mg, 0.027 mol, 38%).

Anal. Calcd for $C_{43}H_{77}INP_3Pt_2\cdot C_7H_8$: C, 45.84; H, 6.54; N, 1.07. Found: C, 45.89; H, 6.37; N, 1.08. $^{31}P\{^1H\}$ NMR (121.38 MHz, C_6D_6): δ 254.1 (t, $^2J_{PP}$ = 104.5 Hz, $^1J_{Pt-P}$ = 4774 Hz), 109.2 (d, $^2J_{PP}$ = 104.5 Hz, $^1J_{Pt-P}$ = 5374 Hz, $^3J_{PP}$ = 57 Hz, $^2J_{Pt-P}$ = 41 Hz). 1H NMR (600 MHz, C_6D_6): δ 7.69 (t, J = 8 Hz, 1H, Ar), 7.14–7.09 (m, 4H, Ar), 7.05 (t, J = 8 Hz, 1H, Ar), 7.00 (m, 1H, Ar), 4.86 (m, 2H, CH₂), 3.95 (sept, J = 7 Hz, 2H, CH), 1.39 (d, J = 7 Hz, 6H, Me), 1.32 (d, J = 7 Hz, 54H, t-Bu), 1.27 (d, J = 7 Hz, 6H, Me). $^{13}C\{^1H\}$ NMR (151 MHz, CDCl₃): δ 146.6 (Ar), 141.6 (d, J = 27 Hz, Ar), 140.4 (Ar), 138.7 (Ar), 128.6 (d, J = 21 Hz, Ar), 128.3 (Ar), 126.7 (d, J = 11 Hz, Ar), 125.8 (Ar), 124.9 (Ar), 122.0 (d, J = 5 Hz, Ar), 61.0 (CH₂), 37.8 (br, quat), 32.5 (br, t-Bu), 28.6 (CH), 27.9 (Me), 25.0 (Me).

Synthesis of 4–Br. Bromophosphine 1–Br (30 mg, 0.080 mol) was dissolved in toluene (4 mL) and added to [Pt(P(t-Bu)₃)₂] (96 mg, 0.160 mol) and stirred overnight (16 h). The dark red reaction mixture was concentrated in vacuo, and the residue was washed with MeCN (10 mL). The crude product was recrystallized from a 1:1 mixture of toluene/MeCN (~3 mL) at -35 °C, affording X-ray-quality red crystals (44 mg, 0.043 mol, 47%).

Anal. Calcd for $C_{43}H_{77}BrNP_3Pt_2\cdot C_7H_8$: C, 47.54; H, 6.78; N, 1.11. Found: C, 47.40; H, 6.70; N, 1.12. $^{31}P\{^1H\}$ NMR (121.38 MHz, C_6D_6): δ 217.1 (t, $^2J_{pp}$ = 129 Hz, $^1J_{p_1-p}$ = 5205 Hz), 102.1 (d, $^2J_{pp}$ = 129 Hz, $^1J_{p_1-p}$ = 5414 Hz, $^3J_{pp}$ = 50.5 Hz, $^2J_{p_1-p}$ = 34 Hz). 1H NMR (600 MHz, CDCl₃): δ 7.46 (t, J = 7 Hz, 1H, Ar), 7.32–7.25 (m, 2H, Ar), 7.19–7.12 (m, 2H, Ar), 7.08 (m, 2H, Ar), 4.78 (m, 2H, CH₂), 3.75 (sept, J = 7 Hz, 2H, CH), 1.30 (d, J = 12 Hz, 54H, t-Bu), 1.24 (d, J = 7 Hz, 6H, Me), 1.18 (d, J = 7 Hz, 6H, Me). $^{13}C\{^1H\}$ NMR (151 MHz, CDCl₃): δ 146.9 (Ar), 140.1 (Ar), 139.7 (Ar), 128.5 (Ar), 128.4 (Ar), 128.3 (Ar), 126.7 (d, J = 11 Hz, Ar), 126.0 (Ar), 124.8 (Ar), 122.1 (d, J = 6 Hz, Ar), 60.2 (CH₂), 38.2 (br, quat), 32.4 (br, t-Bu), 28.7 (CH), 27.7 (Me), 25.0 (Me).

Generation of 6 and Isolation of 7. Fluorophosphine 1–F (35 mg, 0.063 mol) and $[Pt(PPh_3)_4]$ (138 mg, 0.063 mol) were combined in DCM (5 mL) in a vial and stirred for 1 h. $^{31}P\{^1H\}$ NMR spectroscopy revealed two distinct signals with Pt satellites, integrating in a \sim 1:2 ratio with the expected multiplicities. $^{31}P\{^1H\}$

NMR (121.38 MHz, C_6D_6): δ 183.6 (dt, J_{PP} = 205 Hz, J_{PF} = 1060 Hz, J_{Pt-P} = 6550 Hz) and 49.7 (dd, J_{PP} = 205 Hz, J_{PF} = 48 Hz, J_{Pt-P} = 4232 Hz). The yellow and homogeneous solution was concentrated in vacuo, and the resulting residue was washed with cold MeCN (10 mL). The crude solid was then suspended in MeCN (<3 mL) in a 100 mL Schlenk bomb, heated to 80 °C, and cooled to RT overnight, yielding X-ray-quality crystals. The crystalized product (7) had the opposite stoichiometry of what was detected by 31 P{ 1 H} NMR spectroscopy.

Reactivity of 1–Cl with [Pt] in Acetone. Chlorophosphine 1–Cl (100 mg, 0.301 mol) and [Pt(PPh₃)₄] (375 mg, 0.301 mol) were combined in acetone (10 mL) in a vial and stirred for 1 h. The resulting heterogeneous mixture was filtered through a Kimwipe plug in a pipet and concentrated in vacuo. $^{31}P^{1}H^{1}$ NMR spectroscopy revealed two distinct signals with Pt satellites, integrating in a 1:1 ratio. $^{31}P^{1}H^{1}$ NMR (121.38 MHz, C_6D_6): δ 110 (d, $J_{PP} = 509$ Hz, $J_{Pt-P} = 4047$ Hz), 30.5 (d, $J_{PP} = 509$ Hz, $J_{Pt-P} = 2811$ Hz). Other $^{31}P^{1}$ NMR signals include singlets at 122, 24, and 18 ppm. Attempts to purify the major product by $^{31}P^{1}H^{1}$ NMR spectroscopy via recrystallization were unsuccessful; however, one recrystallization from THF/pentane at -35 °C yielded *trans*-PtHCl(PPh₃)₂.

ASSOCIATED CONTENT

Supporting Information

The Supporting Information is available free of charge at https://pubs.acs.org/doi/10.1021/acs.organomet.3c00070.

NMR simulations, methods employed using MestreNova, DFT Calculations, full details on the computational methods, X-ray crystallography, and specifics for the six crystal structures reported (PDF)

DFT SI revised (XYZ)

Accession Codes

CCDC 2191380 and 2236661–2236665 contain the supplementary crystallographic data for this paper. These data can be obtained free of charge via www.ccdc.cam.ac.uk/data_request/cif, or by emailing data_request@ccdc.cam.ac.uk, or by contacting The Cambridge Crystallographic Data Centre, 12 Union Road, Cambridge CB2 1EZ, UK; fax: +44 1223 336033.

AUTHOR INFORMATION

Corresponding Authors

Russell P. Hughes – 6128 Burke Laboratory, Department of Chemistry, Dartmouth College, Hanover, New Hampshire 03755, United States; Email: rphughes46@gmail.com

Matthew F. Cain — Department of Chemistry, University of Hawai'i at Mānoa, Honolulu, Hawaii 96822, United States; orcid.org/0000-0002-0673-5839; Email: mfcain@hawaii.edu

Authors

Preston M. Miura-Akagi — Department of Chemistry, University of Hawai'i at Mānoa, Honolulu, Hawaii 96822, United States

Timothy W. Chapp – Department of Chemistry, Allegheny College, Meadville, Pennsylvania 16335, United States

Wesley Y. Yoshida – Department of Chemistry, University of Hawai'i at Mānoa, Honolulu, Hawaii 96822, United States

Glenn P. A. Yap — Department of Chemistry and Biochemistry, University of Delaware, Newark, Delaware 19716, United States; orcid.org/0000-0003-0385-387X

Arnold L. Rheingold — Department of Chemistry, University of California San Diego, La Jolla, California 92093, United States; orcid.org/0000-0003-4472-8127

Complete contact information is available at:

https://pubs.acs.org/10.1021/acs.organomet.3c00070

Notes

The authors declare no competing financial interest.

ACKNOWLEDGMENTS

M.F.C. thanks the University of Hawai'i at Mānoa (UHM) for laboratory space and in-house maintenance. M.F.C. also thanks the National Science Foundation (NSF) for a CAREER Award (CHE-1847711) and the American Chemical Society Petroleum Research Fund (ACS-PRF: 65352-ND3) for support. Mass spectroscopic data was obtained at UHM on an Agilent 6545 Accurate-Mass QTOF-LCMS (NSF CHE-1532310). T.W.C. acknowledges support from Allegheny College. R.P.H. is grateful to Dartmouth College for computing support and resources. G.P.A.Y. thanks the National Institutes of Health for S10-OD026896A. Elemental analyses were conducted by William Brennessel (University of Rochester).

REFERENCES

- (1) (a) Dillon, K. B.; Mathey, F.; Nixon, J. F. *Phosphorus: The Carbon Copy*; Wiley: New York, 1998. (b) Washington, M. P.; Gudimetla, V. B.; Laughlin, F. L.; Deligonul, N.; He, S.; Payton, J. L.; Simpson, M. C.; Protasiewicz, J. D. Phosphorus Can Also Be a "Photocopy". *J. Am. Chem. Soc.* **2010**, *132*, 4566–4567. (c) Simpson, M. C.; Protasiewicz, J. D. Phosphorus as a Carbon Copy and as a Photocopy: New Conjugated Materials featuring Multiply Bonded Phosphorus. *Pure Appl. Chem.* **2013**, *85*, 801–815.
- (2) Cowley, A. H.; Kemp, R. A. Synthesis and Reaction Chemistry of Stable Two-Coordinate Phosphorus Cations (Phosphenium Ions). *Chem. Rev.* **1985**, *85*, 367–382.
- (3) Gudat, D. Cation Stabilities, Electrophilicities, and "Carbene Analogue" Character of Low Coordinate Phosphorus Cations. *Eur. J. Inorg. Chem.* **1998**, 1087–1094.
- (4) Harrison, J. F.; Liedtke, R. C.; Liebman, J. F. The Multiplicity of Substituted Acyclic Carbenes and Related Molecules. *J. Am. Chem. Soc.* 1979, 101, 7162–7168.
- (5) Bourissou, D.; Guerret, O.; Gabbai, F. P.; Bertrand, G. Stable Carbenes. *Chem. Rev.* **2000**, *100*, 39–92.
- (6) (a) Carbenes: Arduengo, A.J.; Harlow, R.L.; Kline, M. A Stable Crystalline Carbene. *J. Am. Chem. Soc.* **1991**, *113*, 361–363. (b) Phospheniums: Denk, M.K.; Gupta, S.; Ramachandran, R. Aromatic Phosphenium Cations. *Tetrahedron Lett.* **1996**, *37*, 9025–9028.
- (7) Gudat, D. Diazaphospholenes: N-Heterocyclic Phosphines between Molecules and Lewis Pairs. Acc. Chem. Res. 2010, 43, 1307–1316.
- (8) Huynh, H. V. Electronic Properties of N-Heterocyclic Carbenes and Their Experimental Determination. *Chem. Rev.* **2018**, *118*, 9457–9492.
- (9) Lavallo, V.; Canac, Y.; Prasang, C.; Donnadieu, B.; Bertrand, G. Stable Cyclic (Alkyl)(Amino)Carbenes as Rigid or Flexible, Bulky, Electron-Rich Ligands for Transition-Metal Catalysts: A Quaternary Carbon Atom Makes the Difference. *Angew. Chem., Int. Ed.* **2005**, *44*, 5705–5709.
- (10) Soleilhavoup, M.; Bertrand, G. Cyclic (Alkyl)(Amino)Carbenes (CAACs): Stable Carbenes on the Rise. *Acc. Chem. Res.* **2015**, *48*, 256–266
- (11) Frey, G. D.; Lavallo, V.; Donnadieu, B.; Schoeller, W. W.; Bertrand, G. Facile Splitting of Hydrogen and Ammonia by Nucleophilic Activation at a Single Carbon Center. *Science* **2007**, *316*, 439–441.
- (12) (a) Frey, G. D.; Masuda, J. D.; Donnadieu, B.; Bertrand, G. Activation of Si–H, B–H, and P–H Bonds at a Single Nonmetal Center. *Angew. Chem., Int. Ed.* **2010**, *49*, 9444–9447. (b) Martin, D.; Soleilhavoup, M.; Bertrand, G. Stable Singlet Carbenes as Mimics for Transition Metal Centers. *Chem. Sci.* **2011**, *2*, 389–399.

- (13) Rao, B.; Tang, H.; Zeng, X.; Liu, L. L.; Melaimi, M.; Bertrand, G. Cyclic (Amino)(aryl)carbenes (CAArCs) as Strong σ -Donating and π -Accepting Ligands for Transition Metals. *Angew. Chem., Int. Ed.* **2015**, *54*, 14915–14919.
- (14) Power, P. P. Main-Group Elements as Transition Metals. *Nature* **2010**, 463, 171–177.
- (15) Cowley, A. H.; Cushner, M. C.; Lattman, M.; McKee, M. L.; Szobota, J. S.; Wilburn, J. C. The Preparation, Structures, and Reactions of Two-Coordinate Phosphorus Cations. *Pure Appl. Chem.* **1980**, *52*, 789–797.
- (16) Other methods can be found: (a) Burck, S.; Gudat, D.; Nieger, M.; Du Mont, W.-W. P-Hydrogen-Substituted 1,3,2-Diazaphospholenes: Molecular Hydrides. *J. Am. Chem. Soc.* **2006**, *128*, 3946—3955. (b) Dube, J. W.; Farrar, G. J.; Norton, E. L.; Szekely, K. L. S.; Cooper, B. F. T.; Macdonald, C. L. B. A Convenient Method for the Preparation of N-Heterocyclic Bromophosphines: Excellent Precursors to the Corresponding N-Heterocyclic Phosphenium Salts. *Organometallics* **2009**, *28*, 4377—4384.
- (17) Nguyen, M. T.; Gabidullin, B.; Nikonov, G. I. Imino-Stabilised Phosphinidene (or Azaphosphole?) and Some of Its Derivatives. *Dalton Trans.* **2018**, *47*, 17011–17019.
- (18) Zhou, D. Y.; Miura-Akagi, P. M.; McCarty, S. M.; Guiles, C. H.; O'Donnell, T. J.; Yoshida, W. Y.; Krause, C. E.; Rheingold, A. L.; Hughes, R. P.; Cain, M. F. P-Alkynyl Functionalized Benzazaphospholes as Transmetalating Agents. *Dalton Trans.* **2021**, *50*, 599–611.
- (19) Burck, S.; Daniels, J.; Gans-Eichler, T.; Gudat, D.; Nattinen, K.; Nieger, M. N-Heterocyclic Phosphenium, Arsenium, and Stibenium Ions as Ligands in Transition Metal Complexes: A Comparative Elemental and Computational Study. Z. Anorg. Allg. Chem. 2005, 631, 1403–1412
- (20) Although no reports of abstraction reactions with an isolated P–I species could be found, treatment of NHP-derived iodophosphines with molecular iodine or direct synthesis via the redox route in ref 21 produced phosphenium ions: Dube, J. W.; Farrar, G. J.; Norton, E. L.; Szekely, K. L. S.; Cooper, B. F. T.; Macdonald, C. L. B. A Convenient Method for the Preparation of N-Heterocyclic Bromophosphines: Excellent Precursors to the Corresponding N-Heterocyclic Phosphenium Salts. *Organometallics* **2009**, *28*, 4377–4384.
- (21) Reeske, G.; Cowley, A. H. One-Step Redox Route to N-Heterocyclic Phosphenium Ions. *Inorg. Chem.* **2007**, *46*, 1426–1430. (22) (a) Kremlacek, V.; Hyvl, J.; Yoshida, W. Y.; Ruzicka, A.; Rheingold, A. L.; Turek, J.; Hughes, R. P.; Dostal, L.; Cain, M. F. Heterocycles Derived from Generating Monovalent Pnictogens within NCN Pincers and Bidentate NC Chelates: Hypervalency versus Bell-Clappers versus Static Aromatics. *Organometallics* **2018**, *37*, 2481–2490. (b) Tokitoh, N.; Matsumoto, T.; Sasamori, T. Unexpected Cyclization Reaction of an Overcrowded 2-Phosphinophenylmethanimine Derivative leading to the Formation of the First Stable 2-Phospha-2H-Iso-Indole Derivative. *Heterocycles* **2008**, *76*, 981–987.
- (23) Burck, S.; Gudat, D.; Nieger, M.; Benko, Z.; Nyulaszi, L.; Szieberth, D. Spontaneous Phosphorus-Halogen Bond Cleavage in *N*-Heterocyclic Halogenophosphanes Revisted: The Case of P–Br and P–I Bonds. *Z. Anorg. Allg. Chem.* **2009**, *635*, 245–252.
- (24) We speculate the TMSCF₃ is serving as a drying agent for any moisture present in the CsF. CsF alone does not give clean conversion to 1–F nor do other reagents previously used like AgF: Gudat, D.; Haghverdi, A.; Hupfer, H.; Nieger, M. Stability and Electrophilicity of Phosphorus Analogues of Arduengo Carbenes An Experimental and Computational Study. *Chem.—Eur. J.* **2000**, *6*, 3414–3425.
- (25) Fey, N.; Garland, M.; Hopewell, J. P.; McMullin, C. L.; Mastroianni, S.; Orpen, A. G.; Pringle, P. G. Stable Fluorophosphines: Predicted and Realized Ligands for Catalysis. *Angew. Chem., Int. Ed.* **2012**, *51*, 118–122.
- (26) (a) Hoye, T. R.; Hanson, P. R.; Vyvyan, J. R. A Practical Guide to First-Order Multiplet Analysis in ¹H NMR Spectroscopy. *J. Org. Chem.* **1994**, *59*, 4096–4103. (b) Hoye, T. R.; Zhao, H. A Method for Easily Determining Coupling Constant Values: An Addendum to "A

- Practical Guide to First-Order Multiplet Analysis in ¹H NMR Spectroscopy". J. Org. Chem. **2002**, 67, 4014–4016.
- (27) Mislow, K.; Baechler, R. D. Effect of Ligand Electronegativity on the Inversion Barrier of Phosphines. *J. Am. Chem. Soc.* **1971**, 93, 773–774.
- (28) Egan, W.; Tang, R.; Zon, G.; Mislow, K. Barriers to Pyramidal Inversion at Phosphorus in Phospholes, Phosphindoles, and Dibenzophospholes. *J. Am. Chem. Soc.* **1971**, *93*, 6205–6216.
- (29) Dixon, D. A.; Arduengo, A. J.; Fukunaga, T. A new inversion process at Group VA (Group 15) elements. Edge inversion through a planar T-shaped structure. *J. Am. Chem. Soc.* 1986, 108, 2461–2462.
- (30) Arduengo, A. J.; Dixon, D. A.; Roe, D. C. Direct Determination of the Barrier to Edge Inversion at Trivalent Phosphorus: Verification of the Edge Inversion Mechanism. *J. Am. Chem. Soc.* **1986**, *108*, 6821–6823.
- (31) (a) Xu, Y.; Huang, J.; Gabidullin, B.; Bryce, D. L. A Rare Example of a Phosphine as a Halogen Bond Acceptor. *Chem. Commun.* **2018**, *54*, 11041–11043. (b) Siegfried, A. M.; Arman, H. D.; Kobra, K.; Liu, K.; Peloquin, A. J.; McMillen, C. D.; Hanks, T.; Pennington, W. T. Phosphorus···Iodine Halogen Bonding in Cocrystals of Bis(diphenylphosphino)ethane (dppe) and p-Diiodotetrafluorobenzene (p-F4DIB). *Cryst. Growth Des.* **2020**, *20*, 7460–7469.
- (32) Other methods of preparation: Carmalt, C. J.; Lomeli, V.; McBurnett, B. G.; Cowley, A. H. Cyclic Phosphenium and Arsenium Cations with 6π Electrons and Related Systems. *Chem. Commun.* 1997, 2095–2096.
- (33) Jennings, W. B.; Randall, D.; Worley, S. D.; Hargis, J. H. Conformation and Stereodynamics of 2-Dialkylamino-1,3-dimethyl-2,3-dihydro-1*H*-1,3,2-benzodiazaphospholes. An Experimental Nuclear Magnetic Resonance, Ultraviolet Photoelectron, and Theoretical MNDO Investigation. *J. Chem. Soc., Perkin Trans.* 2 1981, 1411–1416
- (34) Burck, S.; Gudat, D.; Nattinen, K.; Nieger, M.; Niemeyer, M.; Schmid, D. 2-Chloro-1,3,2-diazaphospholenes A Crystal Structural Study. *Eur. J. Inorg. Chem.* **2007**, 5112—5119.
- (35) Average P-X bond lengths were reported in refs 23 and 24.
- (36) Waterman, R. σ-Bond Metathesis: A 30-Year Retrospective. *Organometallics* **2013**, 32, 7249–7263.
- (37) Kirlikovali, K. O.; Cho, E.; Downard, T. J.; Grigoryan, L.; Han, Z.; Hong, S.; Jung, D.; Quintana, J. C.; Reynoso, V.; Ro, S.; Shen, Y.; Swartz, K.; Ter Sahakyan, E.; Wixtrom, A. I.; Yoshida, B.; Rheingold, A. L.; Spokoyny, A. M. Buchwald-Hartwig Amination using Pd(I) Dimer Precatalysts Supported by Biaryl Phosphine Ligands. *Dalton Trans.* 2018, 47, 3684–3688.
- (38) Symmetrical halogen bridges: (a) Stambuli, J. P.; Kuwano, R.; Hartwig, J. F. Unparalleled Rates for the Activation of Aryl Chlorides and Bromides: Coupling with Amines and Boronic Acids in Minutes at Room Temperature. *Angew. Chem., Int. Ed.* **2002**, 41, 4746–4748. (b) Durà-Vilà, V.; Mingos, D. M. P.; Vilar, R.; White, A. J. P.; Williams, D. J. Reactivity Studies of $[Pd_2(\mu-X)_2(P(t-Bu)_3)_2]$ (X = Br, I) with CNR (R = 2,6-dimethylphenyl), H₂ and Alkynes. *J. Organomet. Chem.* **2000**, 600, 198–205.
- (39) Bridges with ligands featuring π -delocalization: Dai, W.; Chalkley, M. J.; Brudvig, G. W.; Hazari, N.; Melvin, P. R.; Pokhrel, R.; Takase, M. K. Synthesis and Properties of NHC-Supported Palladium(I) Dimers with Bridging Allyl, Cyclopentadienyl, and Indenyl Ligands. *Organometallics* **2013**, 32, 5114–5127.
- (40) Powers, D. C.; Ritter, T. Bimetallic Redox Synergy in Oxidative Palladium Catalysis. *Acc. Chem. Res.* **2012**, *45*, 840–850.
- (41) Elschenbroich, C. Organometallics, 3rd ed.; Wiley-VCH, 2006.
- (42) Farr, J. P.; Wood, F. E.; Balch, A. L. Head-to-Head and Head-to-Tail Isomers of Binuclear Complexes of Platinum(I) and Palladium(I) Involving 2-(Diphenylphosphino)pyridine as a Bridging Ligand. *Inorg. Chem.* 1983, 22, 3387–3393.
- (43) MestReNova v14.2.0-26256; Mestrelab Research S.L.: Santiago de Compostela Spain, 2020.
- (44) Mastrorilli, P.; Nobile, C. F.; Fanizzi, F. P.; Latronico, M.; Hu, C.; Englert, U. (Phosphido)platinum Complexes by Sodium-

Organometallics Article pubs.acs.org/Organometallics

Promoted Reaction of cis-PtCl₂(PHCy₂)₂ - Synthesis and Crystal Structure of [trans-Pt(PCy2H)2(PCy2)Cl], a Rare Example of a Terminal (Phosphido)platinum(II) Complex. Eur. J. Inorg. Chem. 2002, 1210-1218.

- (45) Taylor, N. J.; Chieh, P. C.; Carty, A. J. Platinum Cluster Compounds: X-Ray Structures of Phosphido-bridged Bi- and Tri-Nuclear Complexes with Strong Metal-Metal Bonds Derived from $[Pt(PPh_3)_4]$. J. Chem. Soc., Chem. Commun. 1975, 448–449.
- (46) Gallo, V.; Latronico, M.; Mastrorilli, P.; Nobile, C. F.; Suranna, G. P.; Ciccarella, G.; Englert, U. Synthesis of Phosphido-Bridged Phosphinito Platinum(I) Complexes by Reaction of cis-PtCl₂(PHCy₂)₂ with Oxygenated Bases - Crystal Structure of $[(PCy_2OMe)Pt(\mu-PCy_2)]_2$ (Pt-Pt). Eur. J. Inorg. Chem. 2005, 4607-4616.
- (47) Mastrorilli, P. Bridging and Terminal (Phosphanido)platinum Complexes. Eur. J. Inorg. Chem. 2008, 4835-4850.
- (48) The complexes described in ref 45 have small deviations from idealized D_{2h} symmetry.
- (49) Leoni, P.; Chiaradonna, G.; Pasquali, M.; Marchetti, F. Dinuclear Phosphido-Bridged Derivatives of Platinum(I). Synthesis and Characterization of $[Pt_2(\mu-P(t-Bu)_2)_2(PH(t-Bu)_2)(L)]$ $[L = P(t-Bu)_2)_2(PH(t-Bu)_2)(L)$ Bu)₂R (R = H, Li, n-Heptyl), CO, η^2 -CS₂]. Inorg. Chem. 1999, 38, 253-259.
- (50) Crabtree, R. H. The Organometallic Chemistry of the Transition Metals, 6th ed.; Wiley, 2014.
- (51) (a) Cotton, F. A.; Gu, J.; Murillo, C. A.; Timmons, D. J. The First Dinuclear Complex of Palladium(III). J. Am. Chem. Soc. 1998, 120, 13280-13281. (b) Powers, D. C.; Ritter, T. Bimetallic Pd(III) Complexes in Palladium-Catalysed Carbon-Heteroatom Bond Formation. Nat. Chem. 2009, 1, 302-309.
- (52) Reiner, B. R.; Bezpalko, M. W.; Foxman, B. M.; Wade, C. R. Lewis Acid Catalysis with Cationic Dinuclear Gold(II,II) and Gold(III,III) Phosphorus Ylide Complexes. Organometallics 2016, 35, 2830-2835.
- (53) Arnold, N.; Bertermann, R.; Bickelhaupt, F. M.; Braunschweig, H.; Drisch, M.; Finze, M.; Hupp, F.; Poater, J.; Sprenger, J. A. P. Formation of a Trifluorophosphane Platinum(II) Complex by P-F Bond Activation of Phosphorus Pentafluoride with a Pt⁰ Complex. Chem.—Eur. J. 2017, 23, 5948-5952.
- (54) Bent, H. A. An Appraisal of Valence-Bond Structures and Hybridization in Compounds of the First-Row Elements. Chem. Rev.
- (55) Al-Ohaly, A.-R.; Nixon, J. F. 31P Nuclear Magnetic Resonance Spectroscopic Studies on some Zerovalent Platinum Phosphine Complexes. Inorg. Chim. Acta 1981, 47, 105-109.
- (56) Tungsten: Schmiedeskamp, B.K.; Reising, J.G.; Malisch, W.; Hindahl, K.; Schemm, R.; Sheldrick, W.S. P-Functionalized Cyclic Phosphinidenemetallophosphoranes $Cp(CO)_2W-P(X)(t-Bu)-P(t-Bu)$ Bu) (X = Cl, H): Direct Formation from Metallophosphines and Transformation Reactions. Organometallics 1995, 14, 4446-4448.
- (57) Rhodium: Scheetz, P. M.; Glueck, D. S.; Rheingold, A. L. Rhodium-Catalyzed Isomerization of a Bis(secondary phosphine) to an Unsymmetrical Diphosphine via P-C Cleavage and P-P and C-H Bond Formation. Organometallics 2017, 36, 3387-3397.
- (58) (a) Bender, R.; Braunstein, P.; Jud, J.-M.; Dusausoy, Y. Comparison of Two Strategies toward the Syntheses of Platinum Mixed-Metal Clusters. Reactivity of Linear M-Pt-M and Mn-Pt-Mn Complexes. X-ray Crystal Structures of $Pt_2M_2(\eta^5-C_5H_5)(\mu_3-\mu_3)$ $CO)_2(\mu-CO)_4(PEt_3)_2$ with M = Cr, Mo, and W. Inorg. Chem. 1984, 23, 4489-4502. (b) Packett, D. L.; Jensen, C. M.; Cowan, R. L.; Strouse, C. E.; Trogler, W. C. Syntheses, Structures, and Mechanism of Formation of trans-Chlorohydrobis(trimethylphosphine)plantium-(II) and trans-Dihydrobis(trimethylphosphine)platinum(II). Energetics of Cis-Trans Isomerization. Inorg. Chem. 1985, 24, 3578-3583.
- (59) Related example of oxidative addition of HCl to PtL₂: Blug, M.; Le Goff, X.-F.; Mezailles, N.; Le Floch, P. A 14-VE Platinum(0) Phosphabarrelene Complex in the Hydrosilylation of Alkynes. Organometallics 2009, 28, 2360-2362.

- (60) Gudat, D.; Haghverdi, A.; Nieger, M. Complexes with phosphorus analogues of imidazoyl carbenes: unprecedented formation of phosphenium complexes by coordination induced P-Cl bond heterolysis. J. Organomet. Chem. 2001, 617-618, 383-394.
- (61) Caputo, C. A.; Brazeau, A. L.; Hynes, Z.; Price, J. T.; Tuononen, H. M.; Jones, N. D. A Cation-Captured Palladium(0) Anion: Synthesis, Structure, and Bonding of [PdBr(PPh₃)₂]⁻ Ligated by an N-Heterocyclic Phosphenium Cation. Organometallics 2009, 28,
- (62) Languérand, A.; Barnes, S. S.; Belanger-Chabot, G.; Maron, L.; Berrouard, P.; Audet, P.; Fontaine, F.-G. [(IMes)₂Pt(H)-(ClBC₅H₄SiMe₃)]: a Borabenzene-Platinum Adduct with an Unusual Pt-Cl-B Interaction. Angew. Chem., Int. Ed. 2009, 48, 6695-6698.
- (63) In two separate cases using a PNP pincer, azaphospholene formation was accompanied by P-Ph bond cleavage and transfer of the Ph unit to Pd(II) or Pt(II): (a) Kunchur, H. S.; Radhakrishna, L.; Pandey, M. K.; Balakrishna, M. S. Novel approach to benzo-fused 1,2azaphospholene involving a Pd(II)-assisted tandem P-C bond cleavage and P-N bond formation reaction. Chem. Commun. 2021, 57, 4835-4838. (b) Kunchur, H. S.; Balakrishna, M. S. Platinum Assisted Tandem P-C Bond Cleavage and P-N Bond Formation in Amide Functionalized Bisphosphine o-Ph2PC6H4C(O)N(H)-C₆H₄PPh₂-o: Synthesis, Mechanistic, and Catalytic Studies. *Inorg.* Chem. 2022, 61, 857-868.

□ Recommended by ACS

Overview of the Synthesis and Catalytic Reactivity of Transition Metal Complexes Based on C=P Bond Systems

Aleksandra Ziółkowska, Łukasz Ponikiewski, et al.

MARCH 20, 2023

ORGANOMETALLICS

READ Z

Reactions of PNCNP and POCOP Pincer Platinum Hydride Complexes with Phenylacetylene and Carbon Disulfide: The Influence of the Pincer Backbone on the Structures of Uns...

Jiarui Chang, Xuenian Chen, et al.

FEBRUARY 28, 2023

ORGANOMETALLICS

READ Z

Improved Trianionic Pincer Ligand Synthesis for Cyclic **Polymer Catalysts**

Vineet K. Jakhar, Adam S. Veige, et al.

MARCH 29, 2023 ORGANOMETALLICS

READ [7

Synthesis of CAAC Complexes by Oxidative Addition of 2-Chloro-3,3-dimethyl-N-ethylindoleninium Cations to **Carbonylmetalates and Subsequent Transmetalation**

Sebastian Termühlen, F. Ekkehardt Hahn, et al.

MARCH 13, 2023

ORGANOMETALLICS

READ Z

Get More Suggestions >